Design, Control and Implementation of CoCoA: A Human-Friendly Autonomous Service Robot

by

Gökay Çoruhlu

Submitted to the Graduate School of Sabancı University
in partial fulfillment of the requirements for the degree of
Master of Science

Sabancı University

August, 2014

Design, Control and Implementation of CoCoA:

A Human-Friendly Autonomous Service Robot

APPROVED BY:

Assoc. Prof. Volkan Patoğlu
(Thesis Advisor) .....

Assoc. Prof. Esra Erdem .....

Assoc. Prof. Kemalettin Erbatur .....

DATE OF APPROVAL: .....

Design, Control and Implementation of CoCoA: A Human-Friendly Autonomous Service Robot

Gökay Çoruhlu

ME, Master's Thesis, 2014

Thesis Supervisor: Assoc. Prof. Volkan Patoğlu

Keywords: Service Robotics, Human-Friendly Robot Design, Holonomic Mobile Base, Passive Velocity Field Control, Mobile Manipulation

Abstract

The growing demand to automate everyday tasks combined with the rapid development of software technologies that can furnish service robots with a large repertoire of skills, are driving the need for design and implementation of human-friendly service robots, i.e., safe and dependable machines operating in the close vicinity of humans or directly interacting with them in social domains. The technological shift from classical industrial robots utilized in structured factory floors to service robots that are used in close collaboration with humans introduces many demanding challenges to ensure safety and autonomy of operation of such robots.

In this thesis, we present mechanical design, modeling and software integration for motion/navigation planning, and human-collaborative control of a human-friendly service robot CoCoA: Cognitive Collaborative Assistant. CoCoA is designed to be bimanual with dual 7 degrees-of-freedom (DoF) anthropomorphic arms, featuring spherical wrists. Each arm weighs less than 1.6 kg and possesses a payload capacity of 1 kg. Bowden-cable based transmissions are used for the arms to enable grounding of motors and this arrangement results in lightweight arms with passive back-driveability. Thanks to passive back-driveability and low inertia of its arms, the operation of CoCoA is guaranteed to be safe not only during physical interactions, but also under collisions with the robot arms. The holonomic base of CoCoA possesses four driven and steered wheel modules and is compatible with wheelchair accessible environments. CoCoA also features a single DoF torso, and dual one DoF grippers, resulting in a service robot with a total of 25 active DoF.

The dynamic/kinematic/geometric models of CoCoA are derived in open source software. Inverse kinematics, stable grasp, kinematic reachability and inverse reachability databases are generated for the robot to enable computation of kinematically-feasible collision-free motion/grasp plans for its arms/grippers and navigation plans for its holonomic base, at interactive rates. For the real-time control of the robot, motion/navigation plans characterizing feasible joint trajectories are passed to feedback controllers dedicated to each joint. The joint space control of each joint is implemented in hardware, while communication/synchronization among different DoF is ensured through EtherCAT/RS-485 fieldbuses running at high sampling rates. To comply with human movements under physical interactions and to enable human collaborative contour tracking tasks, CoCoA also implements passive velocity field control that guarantees user safety by ensuring passivity of interaction with respect to externally applied forces.

The feasibility of the design and the applicability of the overall planning and control framework are demonstrated through dynamic simulations and physical implementations of several service robotics scenarios.

Güvenli Servis Robotu CoCoA'nın İnsan Uyumlu Tasarımı, Kontrolü ve Hayata Geçirilmesi

Gökay Çoruhlu

ME, Master Tezi, 2014

Tez Danışmanı: Doç. Dr. Volkan Patoğlu

Anahtar Kelimeler: Servis Robotları, İnsan Uyumlu Robot Tasarımı, Holonomik Gezgin Taban, Pasif Hız Alanı Kontrolü, Mobil Manipülasyon

Özetçe

Günlük görevlerin otomatikleştirilmesine yönelik gereksinimin artışı ve geniş beceri dağarcığına sahip servis robotlarını destekleyen yazılım teknolojilerindeki hızlı gelişme, insan uyumlu servis robotlarına olan ihtiyacı arttırmıştır. İnsan uyumlu servis robotları, insanların yoğun olarak yer aldığı sosyal alanlarda, insanlarla doğrudan fiziksel etkileşim içinde çalışmaya elverişli olarak tasarlanmış emniyetli ve güvenilir robot sistemleridir. Özel yapılandırımış fabrikalardaki klasik endüstriyel robotlardan, insanlar ile işbirliği içinde kullanılan robotlara doğru olan teknolojik yönelim, robotların otonomisini ve güvenli tasarımını araştırma konuları arasında ön plana çıkarmaktadır.

Bu tezde, güvenli servis robotu CoCoA'nın mekanik tasarımı, hareket/ seyrüsefer planlamaları için modelleme ve yazılım entegrasyonu ve insan ile güvenli bir şekilde çalışmasına imkan sunan kontrol mimarisi yer almaktadır. CoCoA iki elini de kullanabilecek şekilde, insan anatomisine uygun 7 serbestlik dereceli kollara ve küresel bileklere sahip olacak şekilde tasarlanmıştır. Her bir kol 1.6 kgdan daha hafif olup, 1 kg yük taşıyabilme kapasitesine sahiptir. Kollarda motorların gövdeye yerleştirilebilmesine imkan sağlayan Bowden-kablo tahrikli güç aktarım mekanizması kullanılmıştır. Bu tasarım, CoCoA'nın pasif geri sürülebilirliğe ve hafif kollara sahip olmasını mümkün kılmıştır. Pasif geri sürülebilirlik özelliği ve kolların çok düşük atalete sahip olması, CoCoAnın sadece fiziksel etkileşimlerde değil, aynı zamanda robot kollarını içeren çarpışma durumlarında da güvenli olmasını garanti etmektedir. CoCoAnın holonomik tabanı, dört sürülebilir ve yönlendirilebilir tekerlek modülüne sahiptir ve tekerlekli sandalye uyumlu ortamlarda rahatlıkla çalışabilmektedir. Bunlara ek olarak tek serbestlik dereceli gövde ve tek

serbestlik dereceli tutucularıyla, servis robotu CoCoA toplamda 25 aktif serbestlik derecesine sahiptir.

CoCoAnın dinamik/kinematik/geometrik modeli açık kaynak yazılımları kullanılarak türetilmiştir. Ters kinematik, kararlı tutma, kinematik ulaşılabilirlik ve ters kinematik ulaşılabilirlik veritabanları kullanılarak, kollar ve tutucular için kinematik olarak uygun, çarpışmasız hareket/tutma planları, holonomik taban için ise seyrüsefer planları oluşturulmuştur. Robotun gerçek zamanlı kontrolü, eklem yörüngelerini içeren hareket/seyrüsefer planlarının, her ekleme ait kapalı döngü denetleyicilere beslenmesi ile gerçekleştirilmiştir. Her eklemin kontrolü donanım seviyesinde yapılmış ve farklı serbestlik dereceleri arasındaki eş zamanlılık yüksek örnekleme hızında çalışan EtherCAT/RS-485 endüstriyel veriyolu kullanılarak garanti altına alınmıştır. CoCoA'nın fiziksel etkileşim altında insan hareketlerine uyum sağlayabilmesi ve insan ile birlikte rota takip görevlerini yerine getirebilmesi için, pasif hız alan kontrolü (PVFC) uygulanmıştır. Bu kontrol algoritması, dışarıdan uygulanan kuvvetlere karşı pasif oluşu nedeni ile kullanıcıların güvenliğini garanti edebilmektedir.

Planlama ve kontrol mimarisinin uygulanabilirliği dinamik benzetimler ve çeşitli senaryolarının fiziksel olarak uygulanmasıyla gösterilmiştir.

Acknowledgements

First and foremost, I have to thank my research supervisor, Volkan Patoğlu. Without his assistance and dedicated involvement in every step throughout the process, this paper would have never been accomplished. I would like to thank you very much for your support and understanding over these past two years.

Getting through my dissertation required more than academic support, and I have many, many people to thank for listening to and, at times, having to tolerate me over the past two years. I cannot begin to express my gratitude and appreciation for their friendship. Ahmetcan Erdoğan, Ozan Tokatlı, Mustafa Yalçın, Beşir Çelebi and Giray Havur have been unwavering in their personal and professional support during the time I spent at the University. For many memorable times, I must thank Barış Arseven, Hamza Kazanci, Hasan Azgin, Ali Gemci, Ahmet Arat, Ahmet Hancıoğlu and Hayrettin Özkan.

Lastly, I would like to thank my family and Burcu Atay for all their love and encouragement. For my parents who raised me with a love of science and supported me in all my pursuits.

This research is partially supported by TÜBİTAK Grants 111E116, 113M422, and Sabancı University IRP.

Contents

List of Figures

Chapter I

1 Introduction

Development of safe and dependable machines operating in the close vicinity of humans or physically interacting with them has been rapidly gaining importance, such that robots can be successfully integrated into social environments to perform everyday tasks in a wide range of domains, including medical, rehabilitation and service robotics domains. The technological shift from classical industrial robots, which are safely kept away from humans in cages, to human-friendly robots that closely collaborate with humans, posses many major challenges. In particular, inherent safety stands out as an imperative design criterion for human-friendly robots, in addition to other well-known robotic performance criteria [2–5]. Consequently, mechanical design, actuation/transmission selection, and implementation of appropriate control algorithms play crucial roles, while designing inherently safe robotic systems.

1.1 State-of-the-art in Human-Friendly Service Robot Design

Initial studies to improve safety of robotic systems focused on instrumenting high-inertia rigid industrial manipulators with impact sensors and execution monitoring algorithms for software level safety regulation. However, these studies did not consider human-robot collision during robot movements. Industrial robots with high inertia possess high kinetic energies even at low speeds; and in the case of a collision with a human, they may cause severe injuries before the execution monitoring and control algorithms can step in. To quantify the injury risks of undesired collisions that involve humans, Head Injury Criteria (HIC) has been commonly employed in the automotive industry. In 2007, HIC has been introduced to the robotics field to help evaluate safety of robots, when they are in collision with human users [6]. Since HIC is correlated with Maximum Abbreviated Injury Score (MAIS), an anatomy-based coding system that classifies and describes the severity of specific individual injuries, HIC serves as a good predictor for the probability of severe injuries for human-robot collisions [1, 7].

Figure 1.1 presents the correlation between HIC and probability of severe injury, with respect to apparent robot inertia and stiffness [1]. PUMA 560, a rigid industrial robot with high inertia, is presented as a demonstrative example. While Puma 560 is moving with 1 m/s speed, its HIC index is higher than 500, and if collides with a human and this amount of HIC is likely to cause severe injuries with a probability of %90.

A close analysis of HIC index reveals the importance of mechanical design considerations to implement human-friendly robots. As Figure 1.1 il-

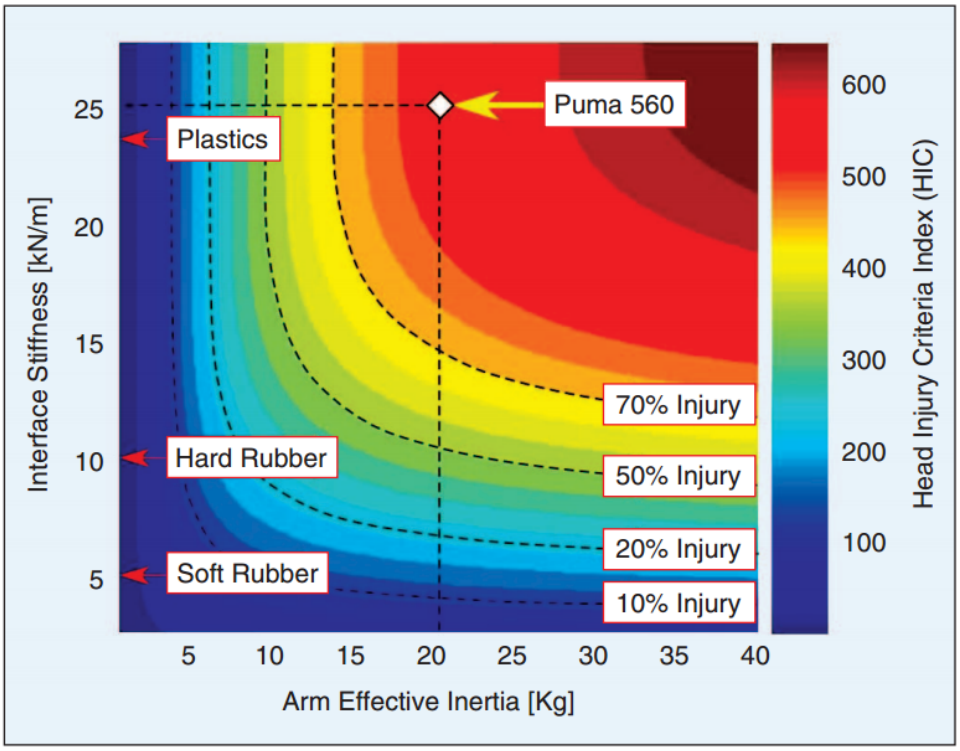

Figure 1.1: Head Injury Criteria (HIC) presented as a function of apparent robot inertia and interface stiffness [1].

lustrates, there are three ways to reduce the injury probability to acceptable levels during an impact: (a) by limiting robot velocity, (b) by covering robot with compliant materials, and (c) by reducing the apparent inertia of the robot. As demonstrated with PUMA 560 example, to ensure safe behaviour of industrial robots even under impacts, their velocities have to be decreased to unacceptably low values. Figure 1.1 also illustrates that industrial robots need to be covered with at least 150 mm layer of compliant rubber-like material in order to reduce their HIC by 5 folds. However, this amount of additional material substantially increases the robot inertia, rendering this solution as infeasible [3].

Consequently, research on human-friendly robot designs focuses on decreasing the apparent inertia of robot arms. Figure 1.2 depicts the state-of-art human-friendly service robots, illustrating the four fundamental design approaches taken to reduce apparent robot inertia during physical interaction with humans.

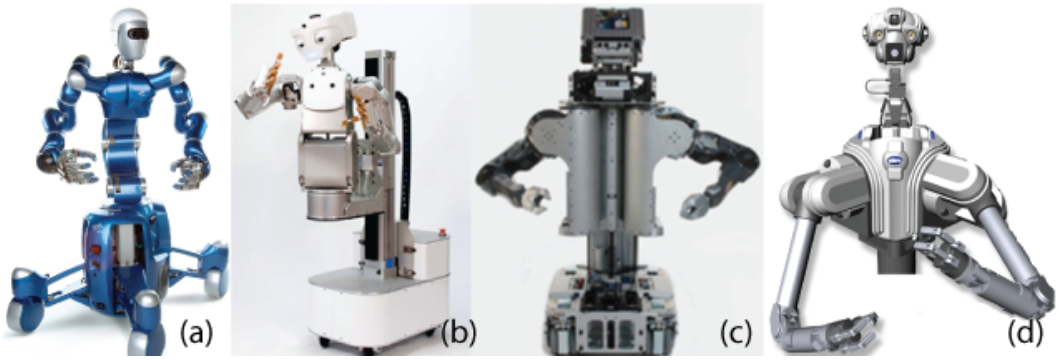

Figure 1.2: State-of-art service robots based on four different design approaches to reduce apparent robot inertia during physical interaction with humans: a) DLR Justin, b) Meka M1, c) Willow Garage PR2, and d) DARPA ARM robot

Figure 1.2(a) illustrates the DLR Justin service robot. The weight of Justin's robot arms is reduced to about 6 kilograms by using carbon fiber links and custom designed light-weight motor harmonic-drive pairs [2, 8]. Torque sensing at each joint plays a crucial role in the control of the DLR arm. Torque sensors measure the joint torque behind the gear-box and enable full-state closed-loop torque control, as well as vibration suppression at real-time with high sampling rates [9]. Thanks to the admittance controller running at high sampling rates, the closed-loop apparent inertia of the robot can be significantly reduced and the DLR arm features high level of active back-drivability while interacting with users. Moreover, the DLR arm has very good torque tracking performance within its control bandwidth.

However, when faced with disturbances that has frequency components over the control bandwidth of the device (e.g., in case of unpredicted impacts with humans), the controller can no longer effectively regulate the device admittance, and open-loop apparent inertia of the device dominates the interaction [10], [11], [12], [13]. Therefore, despite their excellent active backdriveability and interaction performance under closed-loop control, the task speed of admittance controlled robot arms (such as the DLR arm) need to be limited according to their open-loop inertia, to ensure low injury risk under collisions with humans [6].

Figure 1.2(b) presents the Meka M1 service robot, which features Series Elastic Actuation (SEA) at its arms and fingers to ensure safety. The Basic working principle behind SEA is to intentionally add a compliant element (a spring in series) between the non-backdriveable motor group with high transmission ratio and the robot joint [14]. Even though the motor/transmission unit still possesses high inertia and is non-backdriveable, the compliant element decouples the link inertia from the inertia of the motor/transmission unit and guarantees compliance under external forces. Moreover, deflections of elastic joints under external forces can be measured by standard position sensors, which can be used to estimate instantaneous torque levels and implement closed-loop torque control. One of the main advantages of SEA is that, SEA turns the torque control problem into a standard motion control problem. Moreover, SEA features another important advantage; it allows for orders of magnitude higher controller gains be employed by its controllers, compared to explicit force/torque control. Having higher controller gains provides robustness against imperfections in the power transmission; therefore, SEA can be implemented with low cost drive components [15]. The

main difference between joint torque-control (as features in the DLR arm) and SEA is that, thanks to the compliant element, SEA inherently features high-compliance and low apparent inertial (low output impedance) at the frequencies above its control bandwidth. In particularly, under impacts, the series elastic element of SEA dominates the device dynamics and the device displays high compliance/passive back-drivability, while high frequency disturbances are physically filtered out. However, as a trade-off, introducing a soft coupling element significantly lowers the control bandwidth of the robot, rendering SEA as a good option only for slow movements. Moreover, deflections of the elastic element under disturbance forces cannot be controlled; thus, performance and repeatability of SEA is low, making this technology a poor choice for performing precise positioning tasks. To fulfill high precision positioning tasks, SEA robots necessitate extra control algorithms like vision-based control and global sensors to implement those algorithms. From a human-friendly design perspective, unless extra precautions are taken to limit device deflections, SEAs may store substantial amount of potential energy at their elastic coupling elements, which may cause their end-effectors to reach undesirably high velocities and pose danger to humans physically interacting with these devices [3].

Variable Stiffness Actuators (VSA) are introduced as a generalization of series elastic actuators [9, 16], where the stiffness of SEA can be adjusted to match the task requirements. VSAs require two actuators for each joint, such that both the stiffness and position/torque of the device can be regulated. VSAs are controlled with high stiffness to perform precise positioning tasks and with high compliance to perform tasks that require interaction with the environment. In this way, these systems can overcome bandwidth

and precision restrictions of SEAs. However, VSAs possess relatively complex designs since they necessitate two actuators for each degrees of freedom (DoF). From a human-friendly design perspective, similar to SEAs, VSAs can also store potential energy in their compliant elements. Furthermore, adjusting the stiffness of the system can introduces extra external energy, and thus make these systems potentially dangerous to humans, unless appropriate precautions are taken to limit/regulate energy introduced/stored to/in the system.

Figure 1.2(c) depicts the Willow Garage PR2 service robot, which uses a two-level micro-macro actuation approach [17]. Fundamentally, micro-macro actuation is based on using two actuators with different characteristics at each joint of the device: one of these actuators is powerful but slow, and the other one is small but fast [3, 18]. In particular, the powerful but slow actuators (commonly SEAs) are grounded. They are used to compensate for gravitational forces and provide low frequency joint torques. The small but fast (typically direct drive) actuators are located at the joint and are used to improve the control bandwidth of the device. While micro-macro actuation approach can overcome the bandwidth limitations of SEA, the design of such actuators is much more complex. In the Willow Garage PR2 service robot, micro-macro actuation approach is used for the first two joints that are subject to higher gravitational loads and located close to the robot base. In particular, to overcome the gravitational forces, spring-based passive gravity compensation mechanisms are used as the macro actuators. For fast and passively back-driveable movements, direct drive DC motors with capstan transmissions are utilized. Small and light-weight servo motors with low gear reduction ratios are used for all distal joints of PR2 arm, since im-

plementation of macro-micro actuation approach is difficult for these joints, and relatively low torque outputs are required at these joints.

Figure 1.2(d) shows the DARPA ARM robot, which is equipped with two cable-driven Barret Whole Arm Manipulators (WAM) [19]. WAMs are also utilized as a part of the HERB service robot [20]. WAM mounts all its motors to the grounded base; hence, features a light-weight design. The power transmission of WAM is based on cable routing and virtually frictionless capstan transmissions. These design choices ensure that the arm is passively back-driveable. Another novel feature of WAM is that the reduction mechanisms (capstans) are mounted at the joint side, instead of being located at motor side. As a result, the effective elasticity of cable driven system is significantly reduced (by the capstan transmission ratio), while the control bandwidth is significantly increased [21]. WAM possesses high torque control performance and is proper for use at tasks that require physical interaction with humans. However, due to ceramic capstans mounted at the joints, the apparent inertia of WAM relatively high and to ensure human-friendly operation, robot task speed needs to be limited according to the HIC criteria.

Similar to the human-friendly design approaches reviewed above, the design of CoCoA also targets at lowering the apparent inertia of the robot arms during collisions. However, the design of the CoCoA arms is novel in that, the total weight of each arm is kept below 1.6 kg. This (3-4 fold) improvement over the other designs reported in the literature is made possible thanks to Bowden-cable based power transmission that allows the arm actuators to be grounded. The lower apparent inertia of the CoCoA arms renders the robot inherently safe for human collaborative tasks, even in case of collisions with humans or the environment. Furthermore, the arms of the CoCoA feature

passive back-driveability, since power is primarily transmitted by high tension cables and the use of relatively higher friction Bowden-cable shields are kept minimal. Similar to the PR2 arms, the wrists and grippers of CoCoA are implemented using light-weight servo motors with low gear reduction ratios to ensure passive back-driveability. Thanks to a a spherical wrist with collocated joint axes, each arm of CoCoA possesses anthropomorphic 7 DoF. The spherical wrists of CoCoA allow for decoupling of arm kinematics, while human like redundancy of the robot arms significantly extends their dexterity.

Similar to other human-friendly service robot designs, CoCoA features a holonomic base that can operate at wheelchair accessible environments. As in DLR Justin, Mekan M1 and Willow Garage PR2 robot bases, four driven and steered wheel modules are utilized to achieve holonomic base kinematics. This approach is preferable to omni-directional or Mecanum wheel based designs, since better traction (especially at inclined surfaces) and improved localization accuracy can be achieved. From a human-friendly robot design perspective, collisions with the robot base is not of a major safety concern, since the speed of the mobile bases are kept limited to wheelchair speeds, and laser range sensors with very high sampling rates are utilized for obstacle avoidance. However, holonomic mobile bases are passively non-backdriveable and do not comply with human movements under physical interaction. To overcome this limitation, the holonomic base of CoCoA features a passive velocity field controller that enables human collaborative contour tracking tasks, while guaranteeing safety of the user.

1.2 Contributions of the Thesis

- We have performed human-friendly design of CoCoA robot arms, such that the operation of the robot arms is safe even under collisions with human users. Each arm of the robot weighs less than 1.6 kg and features 7 DoF anthropomorphic kinematics with a spherical wrist. The arms utilize Bowden-cable based transmission for the first 5 DoF, allowing actuators to be grounded. Furthermore, thanks to the minimal use of Bowden-cable shields, the arms are passively backdriveable.

- A holonomic base is designed for CoCoA to be compatible with wheelchair accessible environments. The holonomic base utilizes four steered and driven wheels for good traction and localization performance. To enable human collaborative contour tracking tasks and to comply with human movements under physical interaction, a passive velocity field controller that ensures user safety is implemented.

- Kinematic/dynamic/geometric models of CoCoA have been established; and inverse kinematics, stable grasp, kinematic reachability and inverse reachability databases are generated to enable computation of kinematically-feasible collision-free motion/grasp plans for the arms/grippers and navigation plans for the holonomic base at interactive rates. Several use scenarios of CoCoA have been demonstrated through dynamic simulations.

- Motion/navigation plans are computed for kinematically-feasible collision-free joint trajectories. These trajectories have been integrated with

real-time feedback controllers through EtherCAT/RS-485 bus communication. The applicability of the overall planning and control framework is demonstrated through physical implementations of several case studies.

1.3 Structure of the Document

The rest of the thesis is structured as follows:

Chapter II details the kinematic type selection, as well as actuation and transmission selection for the arms, wrists and holonomic base of CoCoA. Implementation details of CoCoA are also covered in this section.

Chapter III covers real-time joint space control of each DoF of CoCoA implemented in hardware through EtherCAT/RS485 bus communication. This chapter also presents the kinematic analysis of the holonomic base of CoCoa and its passive velocity field control for safe human interactions with the base.

Chapter IV presents kinematic/dynamic/geometric models of CoCoA as well as generation of inverse kinematics, stable grasp, kinematic reachability and inverse reachability databases. Computation of kinematically-feasible collision-free motion/grasp plans for the arms/grippers and navigation plans for the holonomic base at interactive rates are also detailed in this chapter.

Chapter V demonstrates the feasibility and applicability of the overall planning and control framework through physical implementations of several case studies.

Lastly, Chapter VI concludes the thesis by summarizing the contributions and discussing future research directions.

Chapter II

2 Mechanical Design of CoCoA Robot

This chapter details the kinematic type selection, as well as the actuation and the transmission selection for the arms, wrists and holonomic base of CoCoA. Implementation and instrumentation of CoCoA are also covered in this section.

2.1 Arms, Wrists and Grippers of CoCoA

Following sections include 7 DoF arm design, implementation and instrumentation details where safety of arm is examined by using HIC criteria.

2.1.1 Kinematic Type Selection of the Arms, Wrist and Gripper

Since CoCoA is designed to work in social environments and is expected to perform everyday chores using tools that are designed for humans users, kinematic properties of the robot arms are selected to closely imitate motion of human arms. Consequently, each arm of CoCoA possesses 7 DoF serial kinematics with a spherical wrist. In particular, the redundant robot arm kinematics is designed to be compatible with human arm kinematics with 3 DoF rotations at the shoulder, 1 DoF rotation at the elbow and 3 DoF rotations at the forearm-wrist of the robot. The redundancy of the arm helps with the dexterity of the robot and the number of inverse kinematic

solutions. The spherical wrist decouples position and orientation kinematics, significantly reducing the time to compute inverse kinematic solutions for the arm.

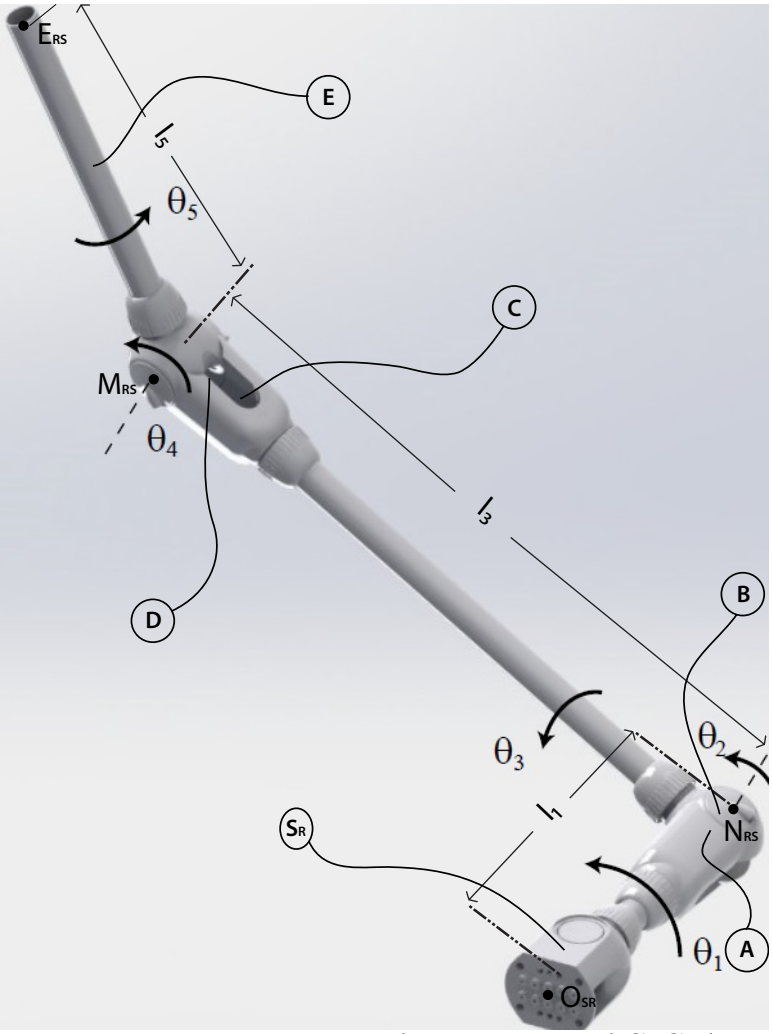

Figure 2.1: Kinematics of 5 DoF arms of CoCoA

Figure 2.1 depicts kinematics of the first 5 DoF of light-weight arms of CoCoA. The link lengths and joint limits for these DoF CoCoA are selected as follows:

$$
\begin{aligned}
l_0 &= 0mm \\
l_1 &= |\overrightarrow{r^{ON}}| = 260mm \\
l_2 &= 0mm \\
l_3 &= |\overrightarrow{r^{NM}}| = 552mm \\
l_4 &= 0mm \\
l_5 &= |\overrightarrow{r^{ME}}| = 396mm
\end{aligned}
$$

$$
\begin{aligned}
-180 < \theta_1 < 180 \\
-90 < \theta_2 < 90 \\
-180 < \theta_3 < 180 \\
-135 < \theta_4 < 45 \\
-180 < \theta_5 < 180
\end{aligned}
\tag{2.1}
$$

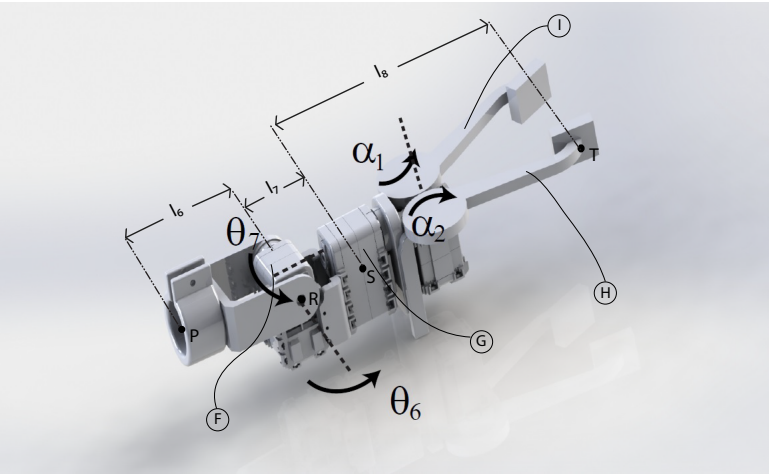

Figure 2.2: Kinematics of 2 DoF wrist and 1 DoF gripper of CoCoA

Figure 2.2 illustrates the kinematics of the wrist and the gripper of CoCoA. The wrist has 2 DoF and, coupled with the last (forearm) DoF of the 5 DoF arm, constitutes a spherical wrist with joint axes intersecting at a single point. This kinematic type selection allows us to decouple the general inverse kinematic problem into two simpler problems: position inverse kinematics and orientation inverse kinematic problems. In particular, the first 4 DoF of the 7 DoF arm can be used for positioning of the end-effector, while the last 3 DoF can be used for assuming the desired orientation. Moreover, thanks to kinematic decoupling, we can obtain analytical solution of inverse kinematic problem (with the use of pseudo-inverse type local optimization approaches to resolve redundancy); this results in significant speeds up in the calculation times.

The link lengths and joint limits for the wrists and grippers of CoCoA are selected as follows:

$$\begin{aligned} l_6 &= |\overrightarrow{r^{PR}}| = 67mm \\ l_7 &= |\overrightarrow{r^{RS}}| = 42mm \\ l_8 &= |\overrightarrow{r^{ST}}| = 140mm \end{aligned} \tag{2.2}$$

$$\begin{aligned} -90 < \theta_6 < 90 \\ -90 < \theta_7 < 90 \\ -60 < \alpha_1 < 60 \\ -60 < \alpha_2 < 60 \end{aligned} \tag{2.3}$$

Finally, a single DoF gripper with two dual flexible fingers are used as the end-effector of each arm.

2.1.2 Actuation and Transmission Selections of the Arms, Wrists and Grippers of CoCoA

Since one of the major design criteria is to reduce the arm inertia to ensure a human-friendly design of CoCoA, actuator and transmission selection plays a vital role in achieving a high performance design. Unlike other service robots in the literature, our design relies on Bowden-cable based transmission for the first 5 DoF of the robot arms. Bowden-cable based transmission enables motors and reduction gears to be mounted on the frame of the robot arms, resulting in significant reductions of arm inertia. Furthermore, unlike cable-based transmission, since routing of Bowden-cables are trivial, very compact joint designs are achievable with this transmission. Since Bowden-cables suffer from friction between the cable and its shield, we have minimized the use of cable shields and utilized tensioned cables as much as possible. As a result, the transmission features relatively low friction losses and arms of CoCoA are passively back-driveable. The links of the arms are made of thin walled aluminum tubes, allowing cable routing to go inside the tubes. Thanks to use of Dyneema polymer material, the Bowden-cables feature higher axial stiffness with lower weight and higher flexibility against bending when compared to steel cables. The overall weight of the 5 DoF Bowden-cable driven arm is less than 1.15 kg. Each of these 5 DoF are actuated by 150 W graphite-brushed DC motors with 7500 rpm rotational speed and 190 mNm torque. Ceramic planetary gearheads with 74:1 reduction ratio are integrated to these motors to achieve joint torques and speeds up to 14 Nm and 100 rpm, respectively.

Figure 2.3 presents the actuation and transmission details for the arms of CoCoA.

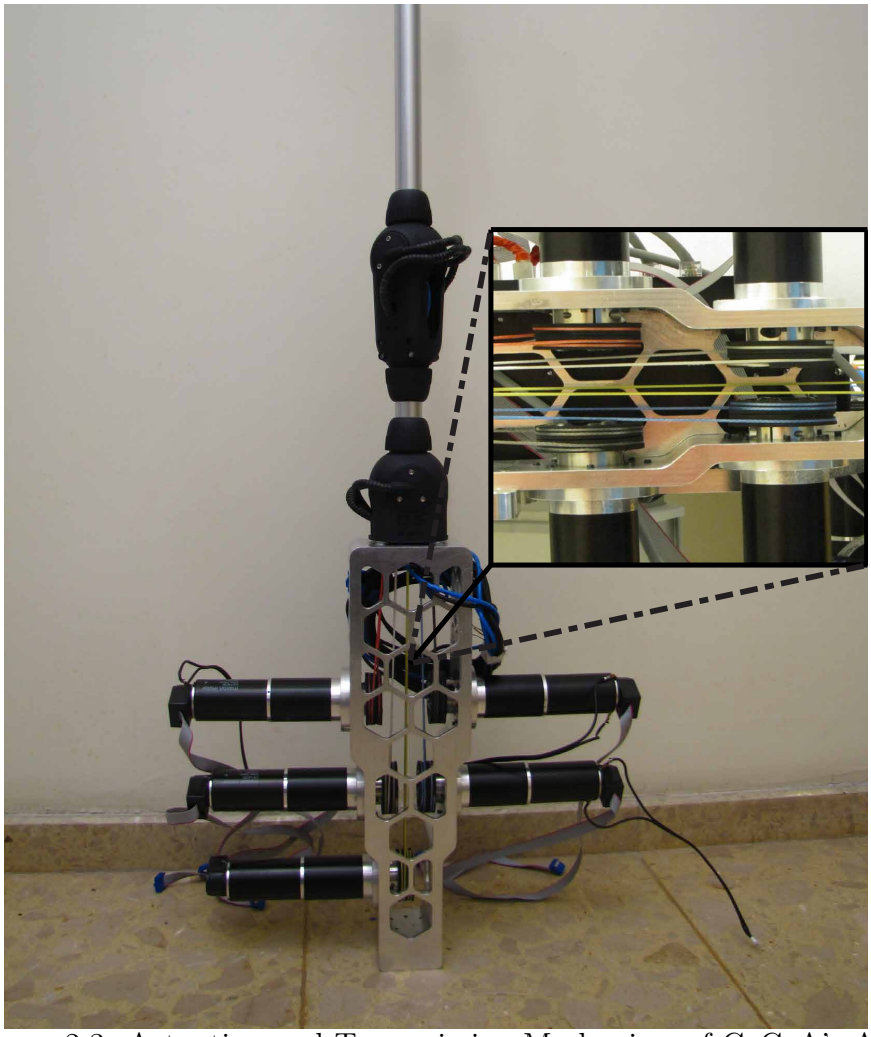

Figure 2.3: Actuation and Transmission Mechanism of CoCoA's Arm

For the last 2 DoF of the arm (the wrist of CoCoA) and the gripper of CoCoA, we have chosen to use lightweight DC motor modules with built-in reduction elements (similar to the wrist/gripper design of PR2 robot [17]). This design decision ensures a light-weight wrist and end-effector design with passive back-driveability, since the torque requirements at these distal joints are relatively low. Note that use of Bowden-cable based transmission for these distal joints results in both higher mass and friction for these last

3 DoF. Each DoF of the wrist and the gripper are actuated with DC motors with 254:1 reduction ratio outputing 55 rpm rotational speed and 2.5 Nm torque. The overall weight of wrist-gripper module is less than 400 g.

Consequently, the total mass of the 7 DoF arm with its spherical wrist and gripper is less than 1600 g. Note that since the elasticity inherent in the transmission decouples the inertia of actuation/reduction unit from the inertia of the arm during an impact, the weight of the arm itself is of crucial importance for human-friendly design of the robot.

Bowden-cable driven pivoting and rotating joints can withstand maximum load torques of 12 Nm and 5 Nm, respectively. Noting that the motors are capable of exceeding these torque values and the distance between the end-effector and the first pivoting joint is 1500 mm, a worst case analysis implies that each arm of CoCoA can manipulate objects that weigh up to 1 kg. Transmission system provides maximum speed of 2 rad/s angular velocity at each joint and that results in a maximum end-effector speed of 2 m/s.

2.1.3 Implementation and Instrumentation of the Arms, Wrists and Grippers of CoCoA

Figure 2.4 presents the final design of CoCoA arms with their actuation/reduction gear units, as well as the placement of dual arms with respect to the robot torso. In this figure, $d_1 = 535$ mm and $d_2 = 75$ mm. Such a placement of the arms allows CoCoA to have 700 mm distance between its shoulders.

The first 5 DoF of arms of CoCoA are instrumented with dual position sensors to enable compensation for elasticity and backlash effects at the

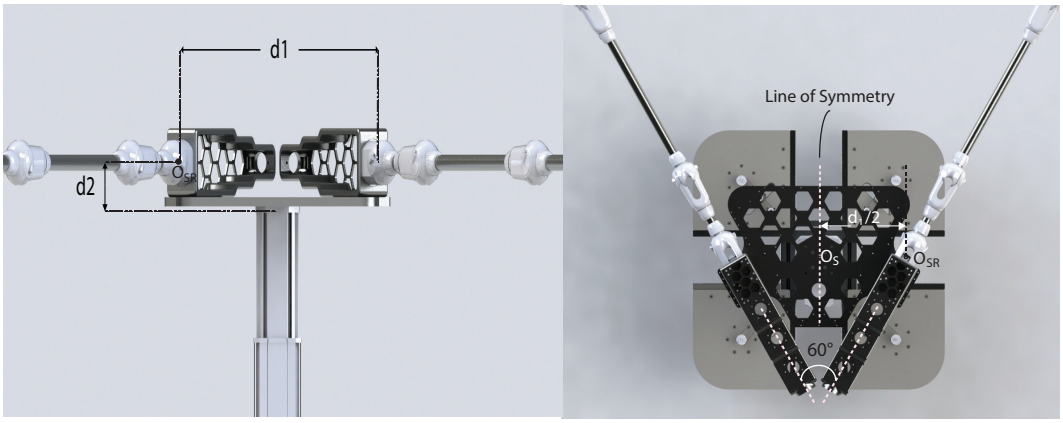

Figure 2.4: Placement of CoCoA's Arms

cable-based transmission. In particular, each DC motor is equipped with optical encoders with 2000 counts per turn (under quadrature decoding), while magnetic incremental angle sensors with a resolution of < 0.07 degrees are located at each joint. The servo motors at the distal 3 DoF are equipped with contactless absolute encoders with 4096 counts per turn (under quadrature decoding).

The motors actuating the Bowden cables are controlled through EtherCAT fieldbus though use of digital positioning controllers for each axis. The actuators of the wrist and the gripper are controlled through RS-485 protocol using their dedicated position controllers. In addition to performing motion control in hardware, both controllers can feed position, velocity and current data back to PC based controller at high sampling rates for execution monitoring and real-time control at joint-level.

2.1.4 Head Injury Criteria for the Arms of CoCoA

HIC value of the arms of CoCoA are calculated to evaluate the safety level of the robot arms under impacts with human users. The derivations in this section closely follows [22] and are included for completeness.

HIC over a time interval $\triangle t_{max}$ is defined as

$$\begin{aligned} HIC(\triangle t_{max}) = max_{t_1,t_2} \left[(\frac{1}{t_2 - t_1} \int_{t_1}^{t_2} \hat{a} \ dt)^{2.5} \ (t_2 - t_1) \right] \\ \text{subject to } t_2 - t_1 \leq \triangle t_{max}, \end{aligned} \tag{2.4}$$

where the head acceleration is represented by $\hat{a}$. The result of this equation is classified as HIC_{15}, if $\triangle t_{max} = 15$ ms, and HIC_{36}, if $\triangle t_{max} = 36$ ms. The head acceleration $\hat{a}$ is defined as $\hat{a} = a/g$, where g is the acceleration of gravity.

Assume that there is a mass-spring-mass model between the robot arm with a total effective inertia of m_1 and an unconstrained human head with a mass of m_2. Moreover, suppose that the stiffness coefficient between those two masses located at x_1 and x_2 is set as k. Under these assumptions, the contact force can be calculated as $k\,(x_1 - x_2)$. We assume that the head is not constrained, which implies that it will eventually lose contact and move away with a constant velocity. Under these assumptions, the normalized head acceleration can be computed as

$$\hat{a} = A \ \sin \omega t, \quad 0 \leq t \leq \pi/\omega \tag{2.5}$$

where

$$\omega = \left[\frac{(m_1 + m_2)k}{m_1 m_2}\right]^{1/2} \quad \text{and} \quad A = \frac{m_1 v_1 \omega}{(m_1 + m_2)g}. \tag{2.6}$$

HIC of the mass-spring-mass system can be calculated by Equation (2.5) to evaluate the integral in Equation (2.4) to perform the maximization. The times t_1 and t_2 that maximize HIC should be symmetric about $\pi/(2\omega)$, since the function is symmetric about $x = \pi/2$. A variable α can be introduced to find the maximum that transforms t_1 and t_2 into $t_1 = (\pi/2 - \alpha)/\omega$ and $t_2 = (\pi/2 + \alpha)/\omega$. At that point HIC can be calculated by the equation

$$HIC(\triangle t_{max}) = 2\, A^{5/2} \omega^{-1} \alpha^{-3/2} (\sin\alpha)^{5/2}, \tag{2.7}$$

where

$$\alpha = min(\alpha^*, \omega \triangle t_{max}/2) \tag{2.8}$$

and α^* is the solution in $[0, \pi/2]$ of

$$3\, \sin\alpha - 5\, \alpha \cos\alpha = 0 \tag{2.9}$$

Equation (2.9) can be solved numerically, since it does not include any parameters of the model. The solution of this equation is approximately equal to $\alpha^* = 1.0528$. To represent full-impact interval, $T = \pi/\omega$ can be used. The switch indicated in Equation (2.8) takes place at $T = 22.38$ ms when numerical value of $\hat{\alpha}$ and interval of 15 ms are used. For short impact times, we can assume that $\alpha = \alpha^*$ and this assumption implies the following conclusions:

HIC_{15} can be rewritten for short-impact times, $T \leq 22.38$ ms as

$$
\begin{aligned}
HIC_{15} &= 1.303\, A^{5/2}/\omega \\
&= 1.303 \left(\frac{k}{m_2}\right)^{3/4} \left(\frac{m_1}{m_1+m_2}\right)^{7/4} \left(\frac{v_1}{g}\right)^{5/2}
\end{aligned} \tag{2.10}
$$

Equation (2.10) can be re-expressed in SI units as follows

$$
HIC_{15} = 0.00433 \left(\frac{k}{m_2}\right)^{3/4} \left(\frac{m_1}{m_1+m_2}\right)^{7/4} v_1^{5/2} \tag{2.11}
$$

$$
HIC_{pub} = 1.016 \left(\frac{k}{m_2}\right)^{3/4} \left(\frac{m_1}{m_1+m_2}\right)^{7/4} v_1^{5/2} \tag{2.12}
$$

To calculate the worst case HIC for the arms of CoCoA, we consider the scenario when the arm is fully extended. Fully extended arm represents the worst case, since the end-effector velocity assumes its maximum value at this configuration. Noting that compliance of the cable based transmission decouples the link dynamics during an impact, the mass of the last link together with the wrist and the end-effector are considered for the HIC calculations. This mass is set as $m_1 = 0.5$ kg, while the mass of the unconstrained head is taken as $m_2 = 4$ kg, as reported in the literature. At this configuration, the Bowden-cable length for the corresponding joint is 770 mm. Considering 107 GPa Young's modulus of Dyneema SK75 material [23], and 2 mm diameter of the Bowden-cable, axial stiffness of the cable can be experimentally determined as $k = 5000$ N/m. Note that the stiffness of the transmission is orders of magnitude lower than the other components and dominates the overall stiffness. Assuming the CoCoA's arm is moving at a speed of $v_1 = 1$ m/s, HIC_{15} can be calculated by Equation (2.11) as

0.0195 s. Furthermore, using Equation (2.12), HIC_{pub} value of the CoCoA's arm can be calculated as 5 $m^{5/2}/s^{-4}$. When maximum allowed speed is used for CoCoA's arm, HIC_{15} is calculated as 0.1925 s and HIC_{pub} is calculated as 45 $m^{5/2}/s^{-4}$.

For comparison, the same calculations are performed for PUMA 560 industrial robot, for which $m_1 = 25$ kg, $m_2 = 4$ kg, $k = 25.000$ N/m, and $v_1 = 1$ m/s. The solutions are $HIC_{15} = 2$ s and $HIC_{pub} = 551$ $m^{5/2}s^{-4}$. These values are more than 100 times greater than the values calculated for the arms of CoCoA.

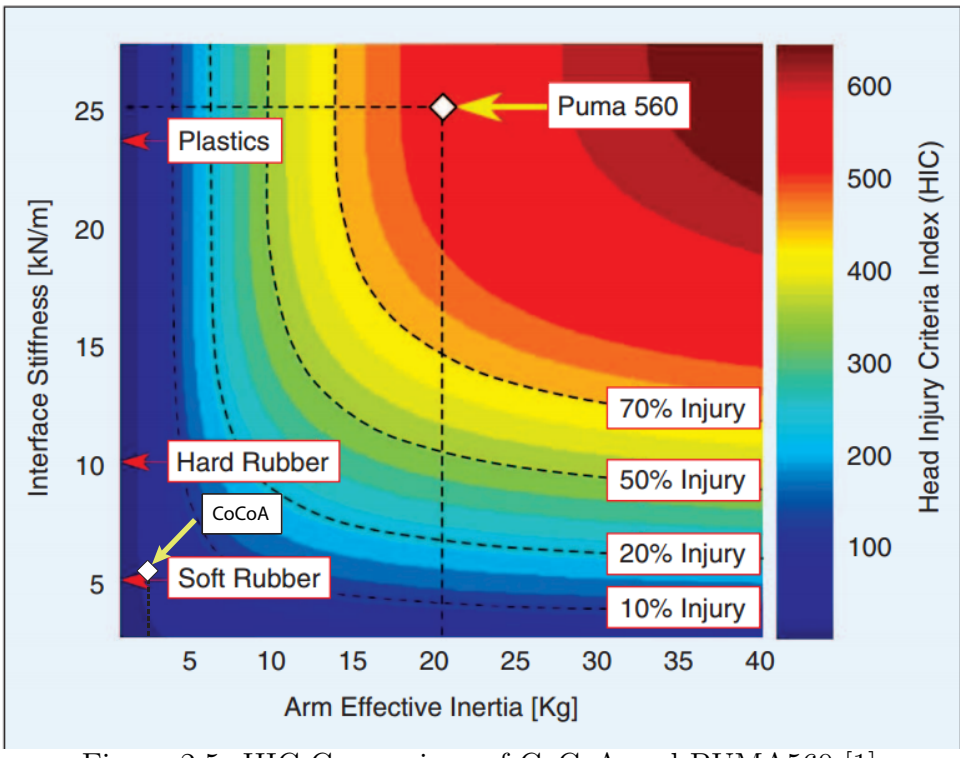

Figure 2.5: HIC Comparison of CoCoA and PUMA560 [1]

Figure 2.5 presents HIC_{pub} values of CoCoA and PUMA560 where the speed of the robots are set to 1 m/s.

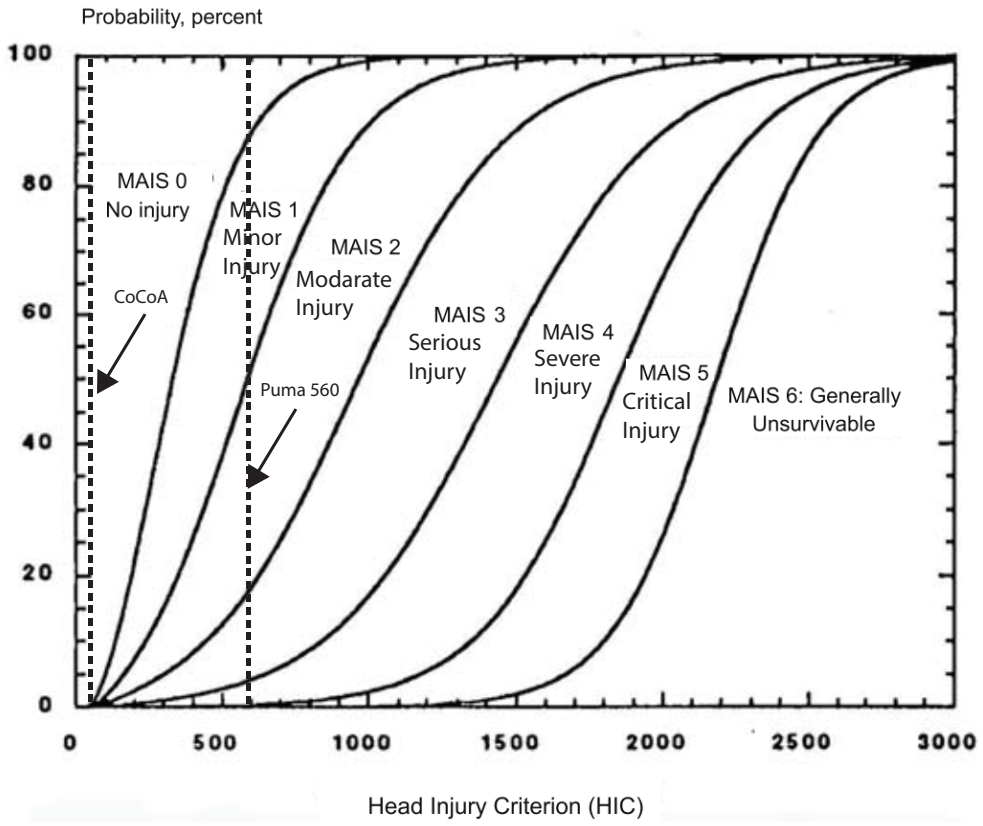

Figure 2.6: HIC of CoCoA at 2.5 m/s End-Effector Speed

Figure 2.6 indicates that even under the worst case impacts with the arms of CoCoA, the probability of moderate to critical injuries are negligible, while Puma560 has a injury risk of 5% for severe injuries, 50% moderate injuries, and 90% minor injuries.

Table 1 presents the specifications for the arms of CoCoA.

Shoulder Yaw Shoulder Pitch Shoulder Roll Elbow Joint Wrist Yaw Wrist Pitch Wrist Roll	360˚ 180˚ 360˚ 135˚ 360˚ 180˚ 180˚
Pay Load	1 kg
Reach	1500 mm
WorkspaceVolume	3.5 m^3
Peak Velocity	2.5 m/s
Peak Acceleration (at endtip with 1-kg load)	4 m/s^2
Weight	
Entire Assembly	6.5 kg
Arm	1.15 kg
Wrist and End-effector	0.4 kg
Size	
Base Height	400 mm
Footprint	0.04 m^2
Actuation	150W graphite-brushed DC motors with 1:74 ceramic planetary gear reduction
Control Interface	EtherCAT
Control Rate	1 kHz
Sensor Resolution	
Joint Side	0.07˚
Motor Side	0.0025˚

Table 1: Specifications of CoCoA's Arms

2.2 Comparison of CoCoA with other designs

Table 2 indicates that CoCoA ensures safety even under collisions, since the arms of CoCoA weigh less than 1.6 kg, which is 3-4 fold improvement compared to the other designs. Moreover, bandwidth and repeatability of CoCoA are adequate to perform mobile manipulation tasks at close to human speeds.

Safety	Back-driveability	Bandwidth	Safety under collision	Arm Weight
Justin	Active	High	Safe under speed limitations	6 kg
Meka-M1	Active	Low	Safe when deflections of SEA are limited	NA
PR2	Passive	High	Safe under speed limitations	5 kg
Darpa ARM	Passive	High	Safe under speed limitations	5.8 kg
CoCoA	Passive	Low	Safe even at the maximum speed	1.6 kg

Performance	Repeatability	PayLoad	Holonomic Base	Anthromorphic
Justin	High	6 kg	✓	✓
Meka-M1	Low	NA	✓	✓
PR2	Intermediate	1.8 kg	✓	✓
Darpa ARM	High	3 kg	✓	✓
CoCoA	Low	1 kg	✓	✓

Table 2: Comparison of CoCoA's Arms with other designs proposed in the literature

2.3 Mobile Base of CoCoA

Design, implementation and instrumentation details of the holonomic base of CoCoA are detailed in the following sections.

2.3.1 Kinematic Type Selection for the Mobile Base of CoCoA

The mobile base of CoCoA is required to be compatible with wheelchair friendly social environments. High maneuverability in tight spaces and good traction ability even on inclined flat surfaces are other important design criteria. Note that due to use of high speed laser range sensors for simultaneous localization and mapping (SLAM), collisions with the mobile base does not pose a critical safety issue when the base speeds are limited to motorized wheel chair speeds.

To ensure good maneuverability and rotations of the robot about its centroid, a holonomic mobile base with omnidirectional movement capability is selected. Among several kinematic arrangements for achieving holonomic base movement, a base kinematics with multiple driven and steered wheels is preferred as the underlying kinematics of the mobile base. Unlike omnidirectional or Mecanum wheels, this kinematic arrangement allows for good traction on flat surfaces with relatively lower level of wheel slip. Even though this kinematic arrangement can be implemented with two driven and steered wheels and a passive wheel, similar to the base designs of other service robots, we have decided to use a redundant arrangement with four driven and steered wheels. The redundancy in actuation and corresponding sensing units is beneficial for improving localization accuracy under dead reckoning, while also enabling smaller actuators be used at each wheel to achieve the desired level of acceleration for the mobile robot. Kinematics based on four driven and

steered wheels has also better performance on inclined and carpet covered surfaces.

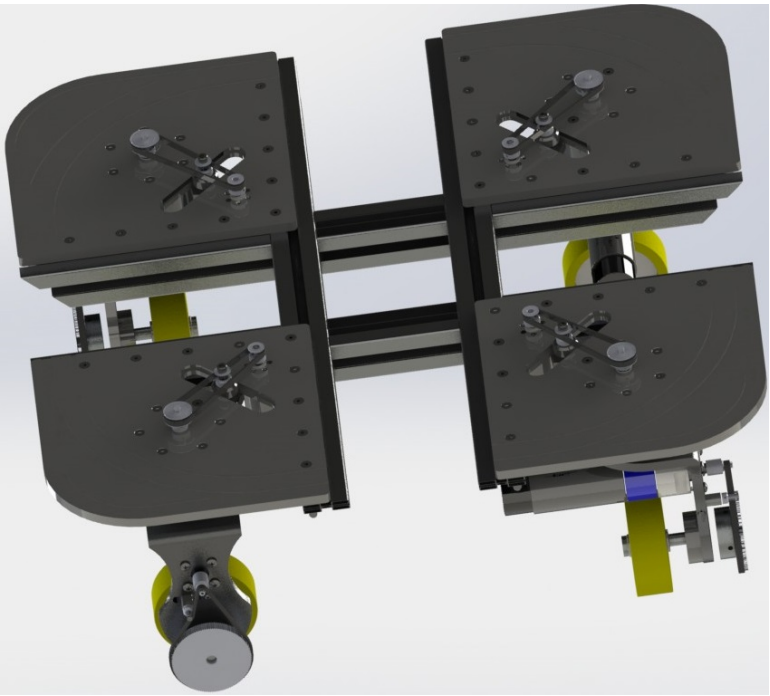

Figure 2.7: Kinematics of Holonomic Base of CoCoA

Figure 2.7 depicts a solid model of the holonomic base of CoCoA. To comply with the regulations of wheelchair compatible structures, the holonomic base is designed to have a square shape with a width of 70 cm and length of 70 cm. The height of the base is 25 cm from the ground. The size of CoCoA allows it to easily navigate through standard social environments (e.g. houses, hospitals, nursing homes), involving doors and elevators.

2.3.2 Design and Implementation of the Mobile Base of CoCoA

Figure 2.8 presents the design of the driven and steered wheel module of the holonomic base. Each wheel module contains two actuators, one for

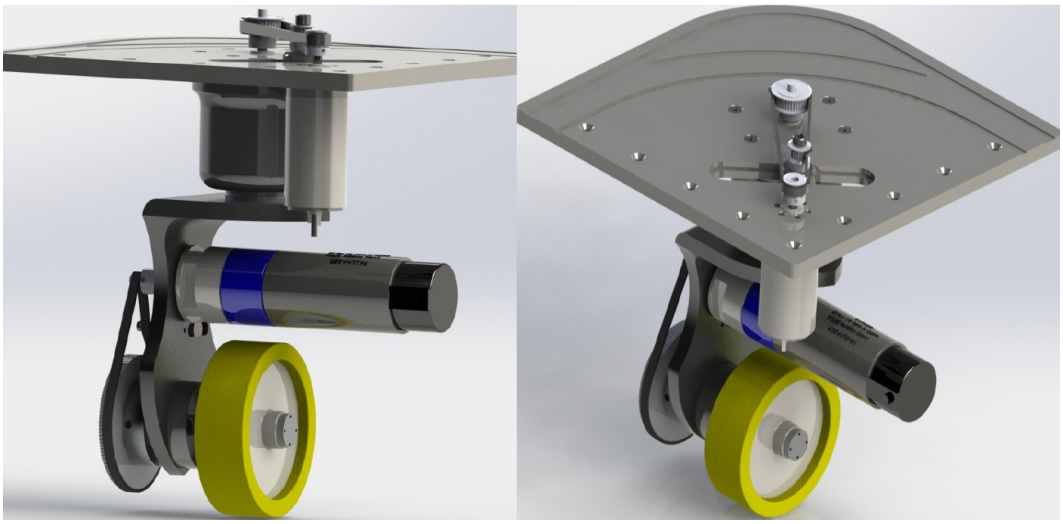

Figure 2.8: CoCoA's Wheel Module

steering and one for driving. We have used 150 W DC motors equipped with 74:1 ratio planetary gearheads for steering. Additionally, the steering transmission features a second layer of 7:3 reduction based on timing belts and pulleys. We have used 200 W EC motors equipped with 44:1 ration planetary gearheads for driving the wheels. The drive transmission also has as second layer of 40:3 reduction based on timing belts and pulleys. The timing belts are intentionally introduced to the drive train to protect the gear motors, as belts add necessary level of elasticity to mechanically filter out impacts that are exerted to the wheels. EC motors are utilized for driving the wheels, since thanks to their built-in hall effect sensors velocity control can be implemented at very high sampling rates. Moreover, due to contact free operation principle, EC motors have higher lifetime than brushed DC motors.

Each motor on the driven and steered wheel module is equipped with optical encoders with 2000 counts per turn resolution (under quadrature de-

coding). In addition to such optical encoders, EC motors are also equipped with hall-effect sensors necessary for their operation. All the motors are controlled through EtherCAT fieldbus thanks to use of digital motion controllers for each axis.

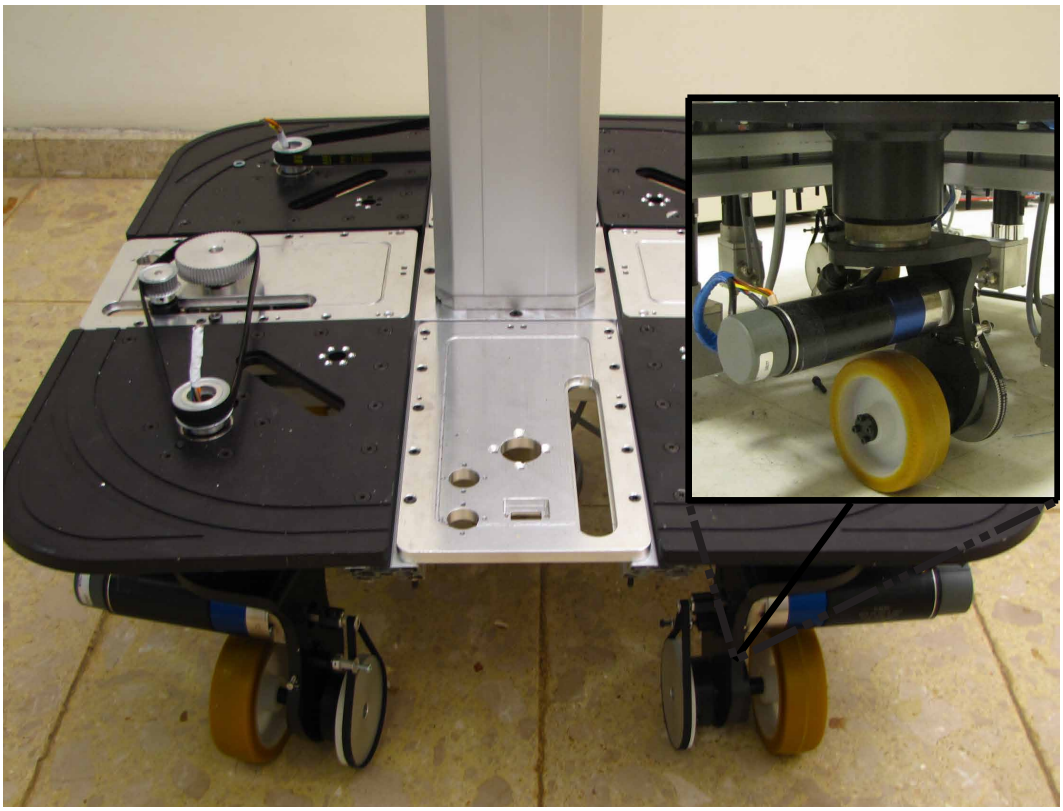

Figure 2.9: Holonomic Base of CoCoA

2.4 Design of the Torso of CoCoA

The arms of CoCoA are attached to its holonomic base through a telescopic pillar with 400 mm stroke. The telescopic pillar can exert 2.5 kN pull/push force with 15 mm/s speed under maximal loading. The stroke of the telescopic pillar is selected to allow CoCoA to grasp objects on the ground, as

well as to manipulate objects located on 1.5-2 m high shelves, commonly encountered in human work spaces.

Figure 2.10 illustrates the shortest and the longest torso posture of CoCoA,

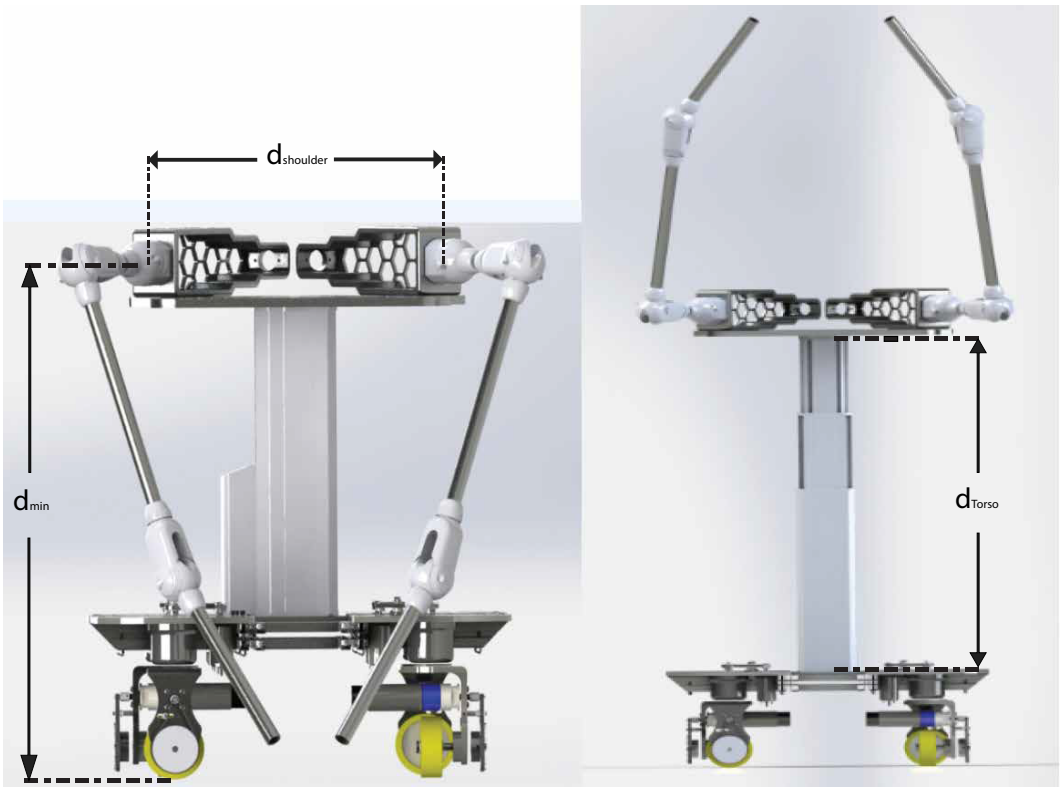

Figure 2.10: Solid Model of the Torso of the CoCoA

where the stroke of the telescopic pillar is limited to 530 mm $\leq d_{Torso} \leq$ 930 mm, minimum height of the arms is 780 mm, and the distance between two shoulders is 540 mm.

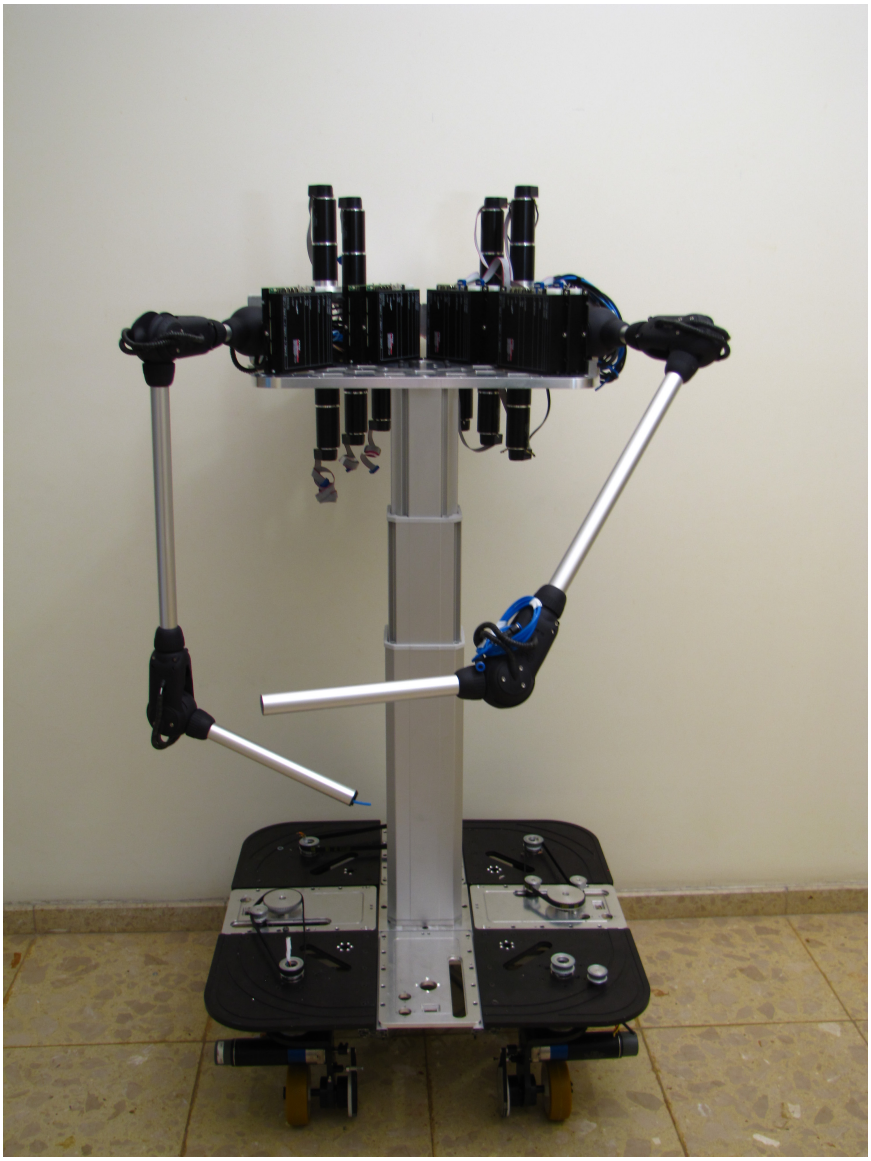

Figure 2.11: Torso of CoCoA

Figure 2.11 illustrates the torso of CoCoA integrated with its arms and holonomic base.

2.5 Final Design of CoCoA

CoCoA is designed to have two arms, a holonomic base and a torso. Each arm of the robot weighs less than 1.6 kg and features 7 DoF anthropomorphic kinematics with a spherical wrist. The arms utilize Bowden-cable based transmission for the first 5 DoF, allowing actuators for these joints to be grounded. Furthermore, thanks to the minimal use of Bowden-cable shields, the arms are passively backdriveable. A holonomic base is designed for CoCoA to be compatible with wheelchair accessible environments. The holonomic base utilizes four steered and driven wheels for good traction and localization performance. The holonomic base and the arms connected to each other by a 400 mm stroke telescopic torso.

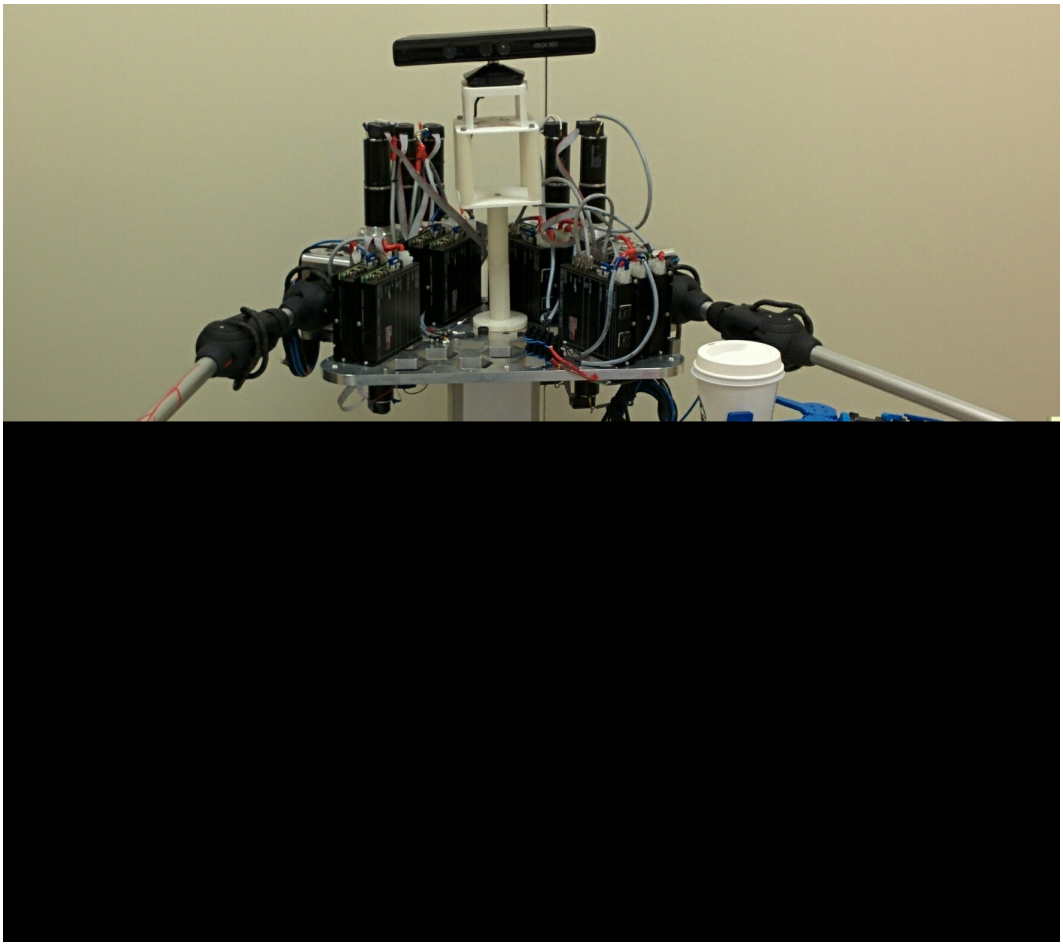

Figure 2.12: Final Design of CoCoA

Figure 2.12 presents the final design of CoCoA that features a single DoF torso, dual 7 DoF arms and 1 DoF grippers, resulting in a service robot with a total of 25 active DoF.

Chapter III

3 Control of CoCoA Service Robot

This chapters details the low-level control of the 7 DoF arms and the holonomic base CoCoA robot. In particular, after a brief review of the arm kinematics, joint level position control of the arms in hardware is explained in detail; afterwards, experimental verification of control performance is presented. Similarly, for the base control, firstly the kinematic model of 8 DoF redundant holonomic base is derived such that, given navigation plans for the base, each DoF of the holonomic base can be controlled at joint space to track this trajectory. Afterwards, passive velocity field control (PVFC) is reviewed and PVFC is implementation for the control of the holonomic base. Simulation results are presented to validate feasibility of contour tracking of the holonomic base with PVFC.

3.1 Kinematics of CoCoA's Arms

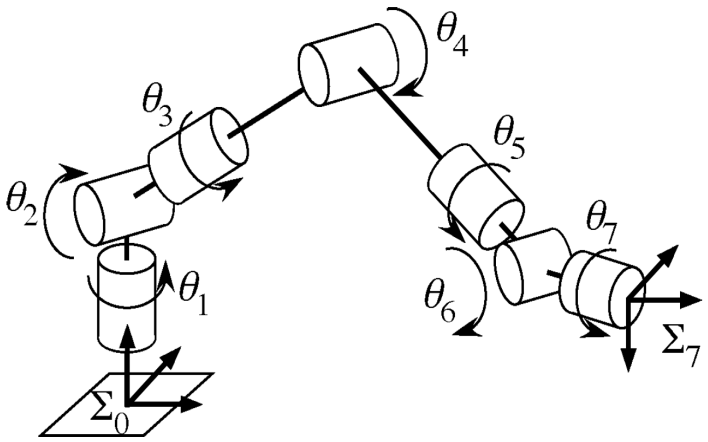

Figure 3.1: Kinematics of CoCoA Arm

As presented in Figure 3.1, each arm of CoCoA features 7 DoF serial kinematics with a spherical wrist. The redundant robot arm kinematics is compatible with human arm kinematics with 3 DoF rotations at the shoulder, 1 DoF rotation at the elbow and 3 DoF rotations at the forearm-wrist of the robot. The redundancy of the arm helps with the dexterity of the robot as it significantly increases the number of inverse kinematic solutions. The spherical wrist decouples position and orientation kinematics; hence, enables analytical solutions to computed for the inverse kinematics for the arm.

In Chapter 4, the kinematics of the arm is defined in XML format and IKFast module of OpenRave software is utilized to calculate the inverse kinematic solutions as well as collision free feasible motion plans for the arms. Note that IKFast module is preferred as it makes use of analytical methods to calculate inverse kinematics at very high rates.

3.2 Control of CoCoA's Arms

Since motion planning modules (also detailed in Chapter 4) provide joint space trajectories for the robot arms to follow, this section only considers joint level control of CoCoA's arms. Control of each joint is implemented on hardware while communication of reference trajectories takes place through an EtherCAT fieldbus. In particular, Maxon EPOS 3 70/10 EtherCAT digital positioning controllers are utilized at each DoF, since these controllers can provide high performance in real-time positioning of synchronized multi-axis systems. To ensure good position tracking performance, Profile Position Mode (PPM) of the digital controller is used, as this mode moves the position of the motor axis from Point A to Point B. Positioning can be performed in relation to the axis home position (absolute) or the actual axis position (relative) [24].

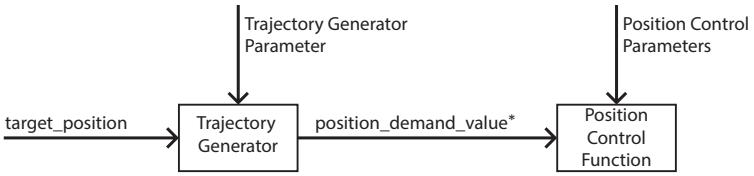

Figure 3.2: Overview of the Profile Position Mode

Figure 3.2 illustrates the general control architecture of EPOS3 70/10 EtherCAT controller PPM. Position demand value, used by Position Control Function, is generated as detailed in the block diagrams presented in Figures 3.3 and 3.4.

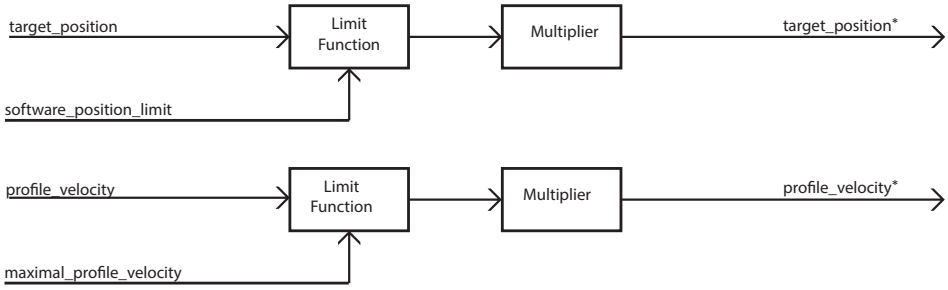

Figure 3.3: Block Diagram of the Position Demand Value

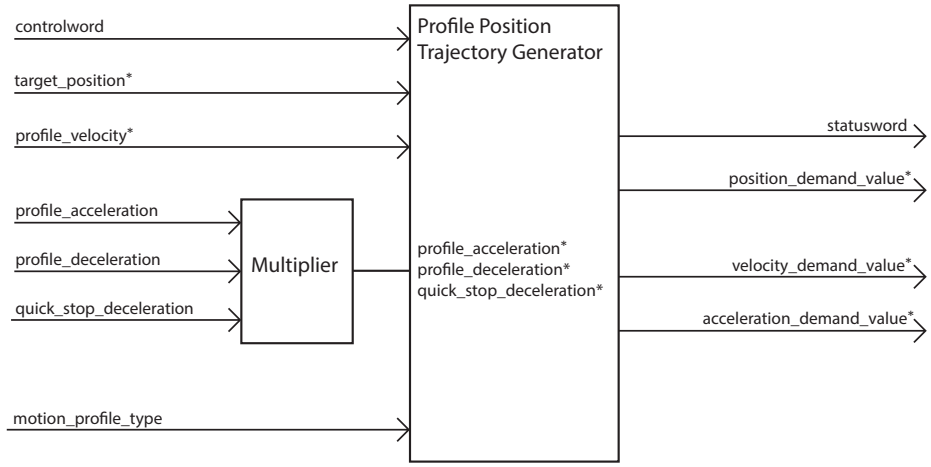

Figure 3.4: Detailed Block Diagram of the Position Demand Value

The position demand value is fed to the position control loop schema as shown in Figure 3.5. Inputs of the control loop are *Target Position* and optional *Position Offset*. Moreover, for feed-forward control, velocity and torque offset can be provided to the control loop.

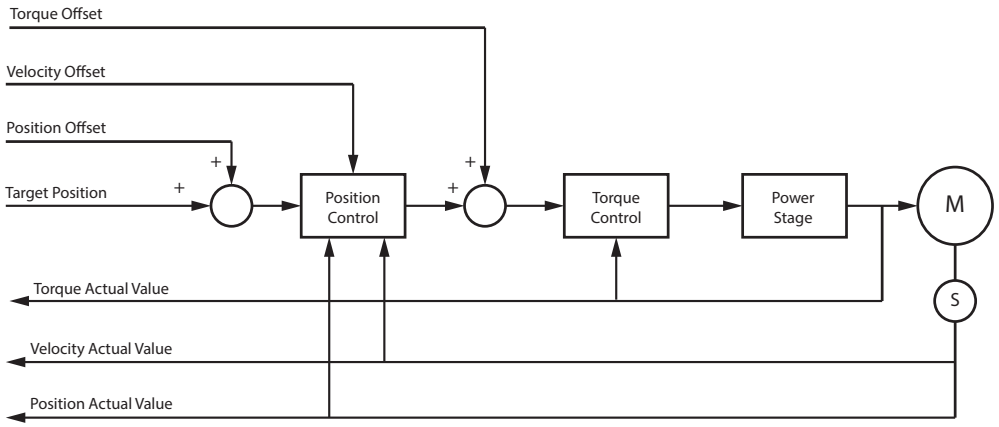

Figure 3.5: Position Control Loop Block Diagram

Sample rate of the PI controller that is used by PPM is 10 kHz while PID control implemented at 1 kHz. We utilize an industrial PC as the master EtherCAT device to communicate with the slave EtherCAT controllers (EPOS 3 controllers) through EtherCAT bus. TwinCAT 3 is used as the communication software with TE1400 TwinCAT Target for MATLAB Simulink add-on, which allows generation of real-time capable modules. By using the Simulink Coder (formerly known as Real-Time Workshop), real-time-capable C or C++ code of block diagrams implemented in Simulink, can be generated. We have used this add-on to generate TcCOM modules that include the input and output behavior of the source Simulink models. When the parameterization process is complete, TwinCAT 3 runtime executes generated modules in real-time and these modules can be integrated with physical controllers [25]. Figure 3.6 illustrates the real-time joint space position control schema.

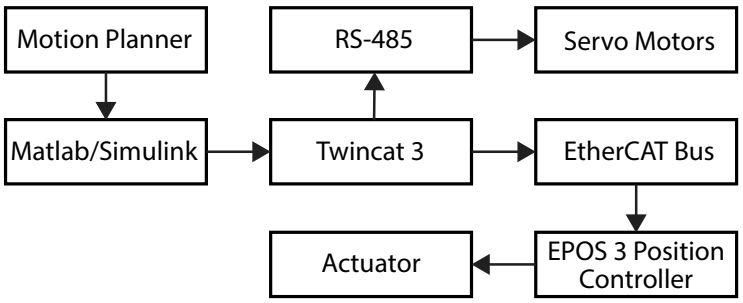

Figure 3.6: Overall of Joint Space Position Control Schema

The position controller implemented using PPM only utilizes a single position sensor, in our case the encoder located at each motor. However, cable driven joints of CoCoA are also equipped with encoders at each joint and the EtherCAT controller offers dual-loop control as an option. Dual-loop control is advantageous since it can compensate for friction, compliance and backlash inherent to the drive chain. In particular, planetary gearheads and Bowden-cables in the power transmission of arm joints introduce parasitic dynamic effects that may induce vibrations and reduce precision of the arms. Utilizing sensory feedback on motor movement as well as the load movement, dual-loop control can effectively compensate for these undesired effects.

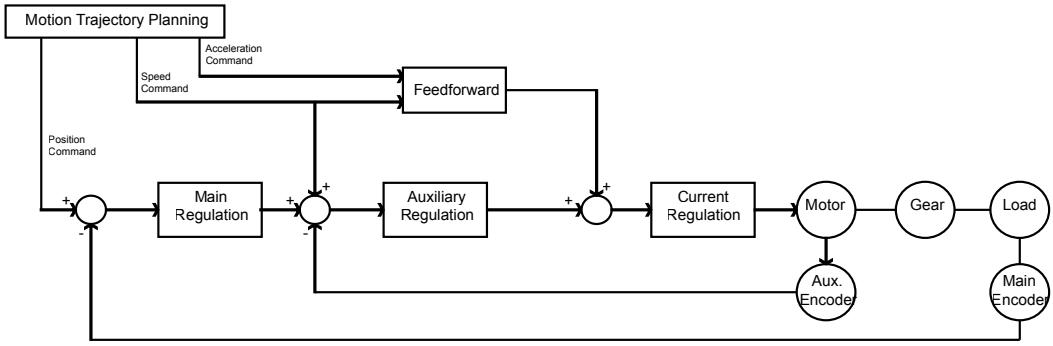

Figure 3.7: Dual-Loop Control Architecture

Figure 3.7 illustrates the dual-loop control mode of the digital EtherCAT controller, where the main regulation module ensures achievement of desired position precision, while the auxiliary regulator compensates for parasitic effects on the transmission and introduces active damping to suppress vibrations.

To evaluate control performance of the arm, we have studied the performance of the digital positioning controller with three distinct reference inputs: unit step unit, ramp input, and joint trajectory generated by a motion planner. Figures 3.8, 3.20 and 3.12 present experimental tracking results recorded during the real-time control of the Bowden-cable driven arm joints for unit step, ramp and trajectory inputs, respectively. Similarly, Figures 3.9, 3.11 and 3.13 illustrate trajectory errors for these inputs where the % RMS tracking error is less than 0.01% for these experiments.

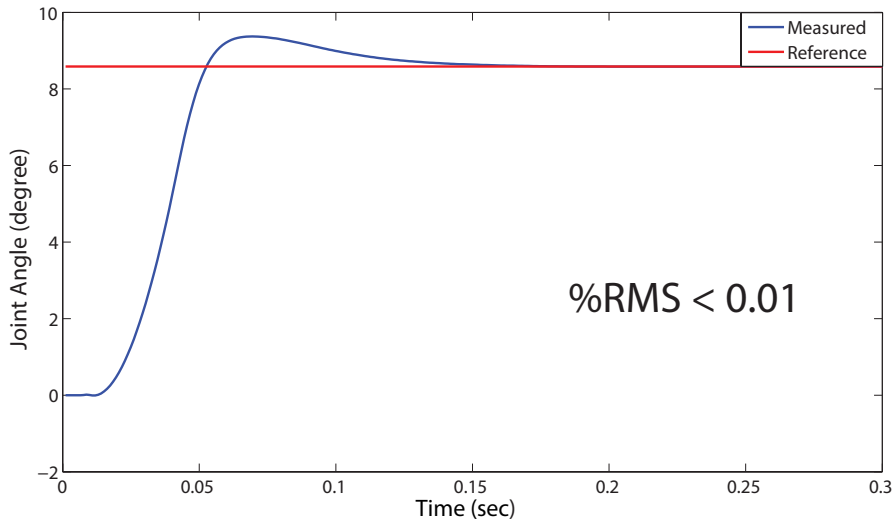

Figure 3.8: Unit Step Response of the Control System

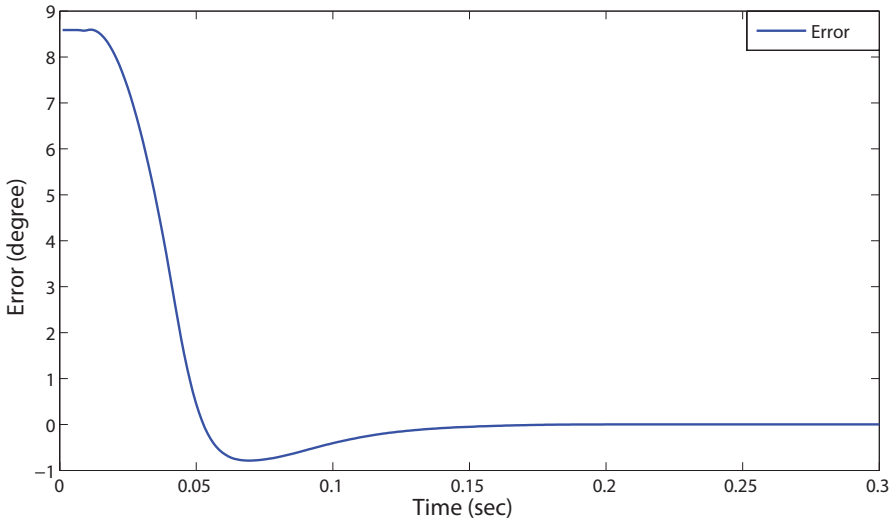

Figure 3.9: Unit Step Error of the Control System

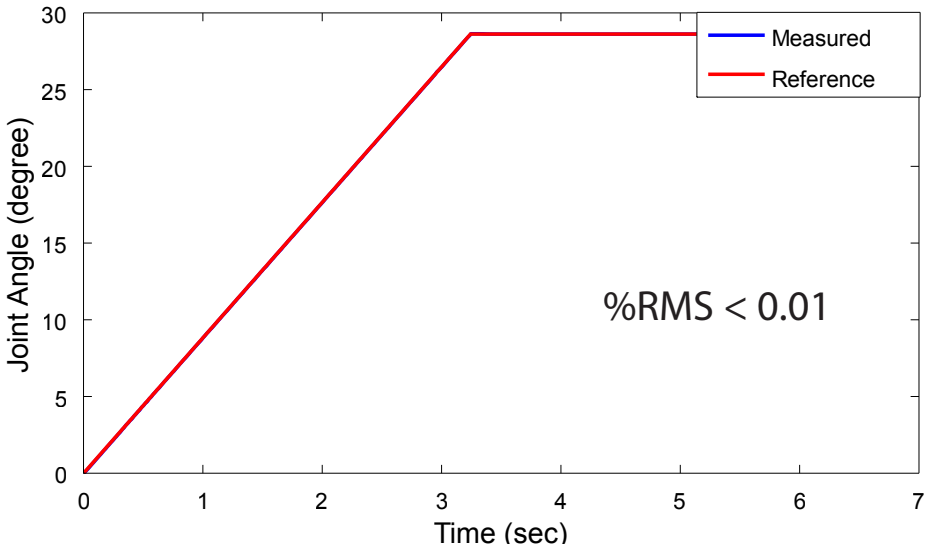

Figure 3.10: Ramp Response of the Control System

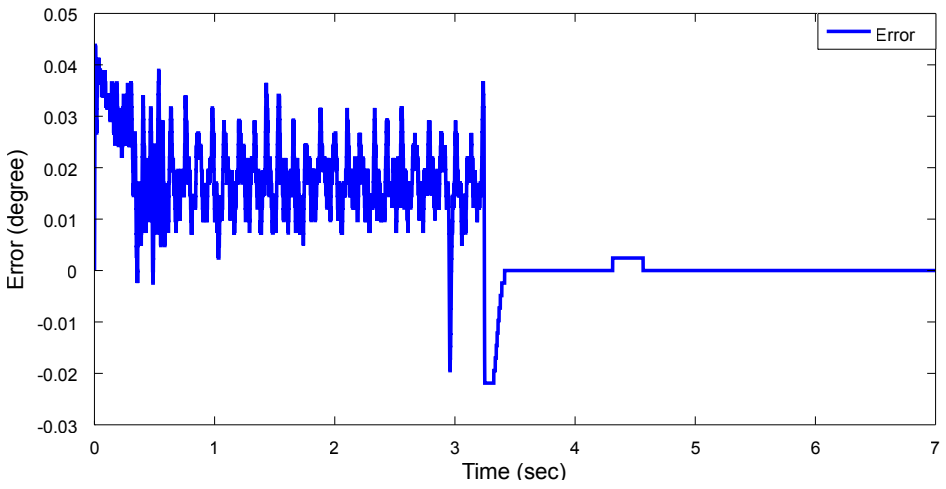

Figure 3.11: Ramp Error of the Control System

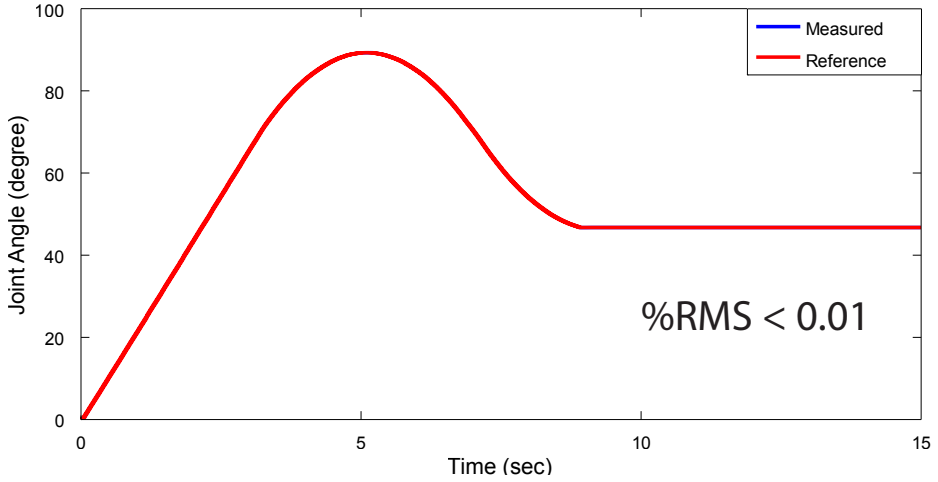

Figure 3.12: Smooth Trajectory Tracking Response of the Control System

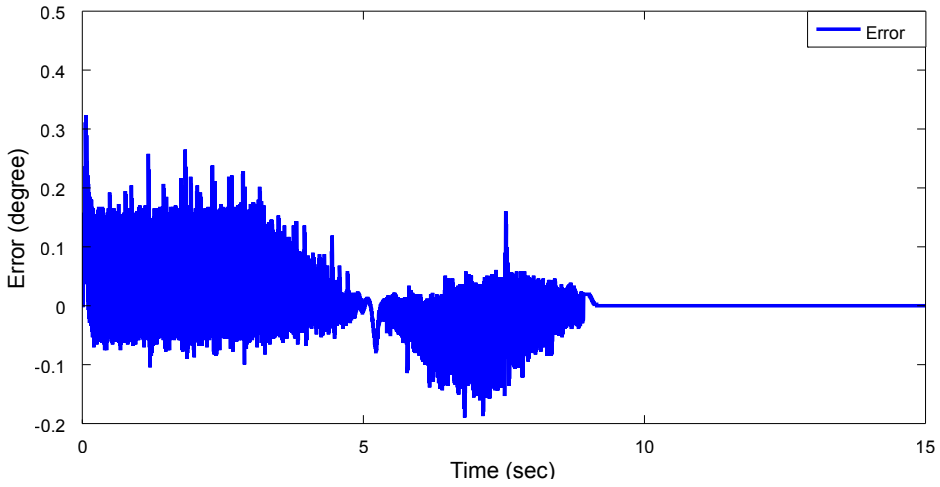

Figure 3.13: Trajectory Tracking Error of the Control System

Real-time control performance of the second and the third joints are also tested and these results are given in Figures 3.14 and 3.16. Corresponding errors are represented in Figures 3.15 and 3.17.

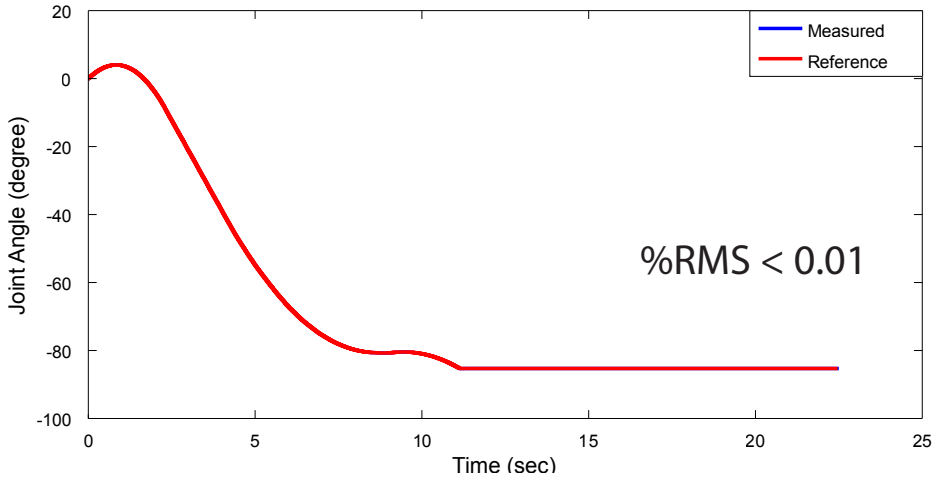

Figure 3.14: Smooth Trajectory Tracking Response of the Second Joint

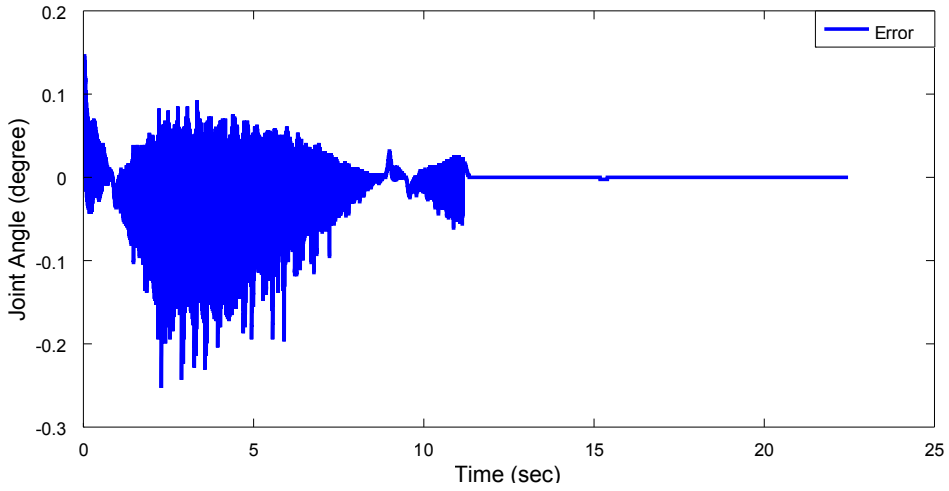

Figure 3.15: Trajectory Error of the Third Joint

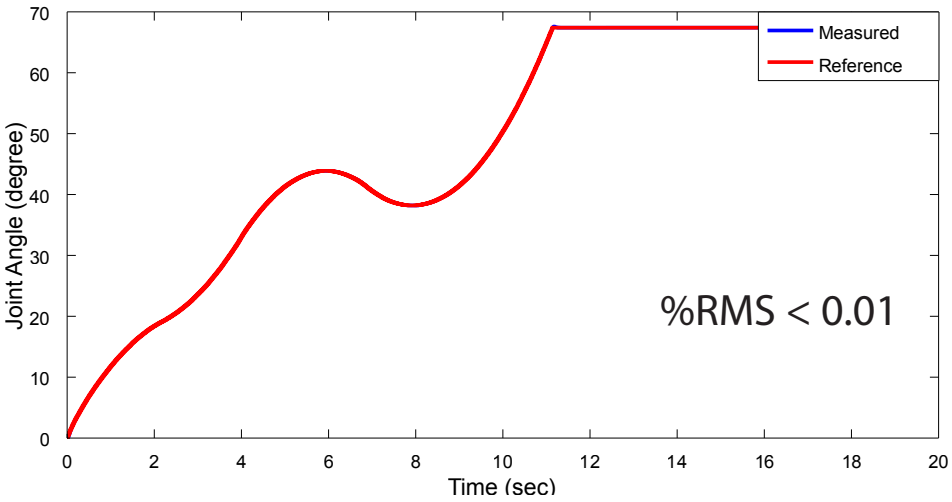

Figure 3.16: Smooth Trajectory Tracking Response of the Third Joint

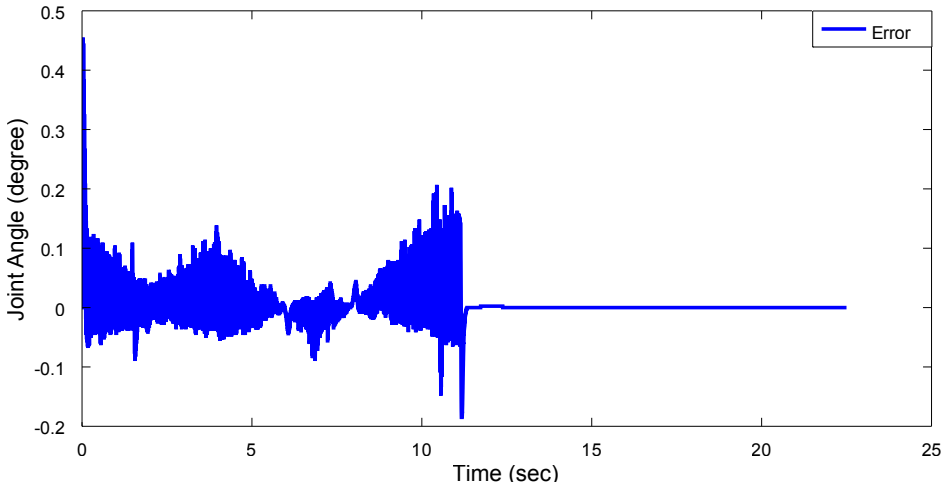

Figure 3.17: Trajectory Error of the Third Joint

3.3 Control of CoCoA's Wrists and Grippers

To actuate the wrist joints, servo motors equipped with integrated controllers are utilized. These controllers feature a compliance mode that implements some sort of rudimentary impedance control (a virtual spring). To set the control flexibility, the motor compliance is used.

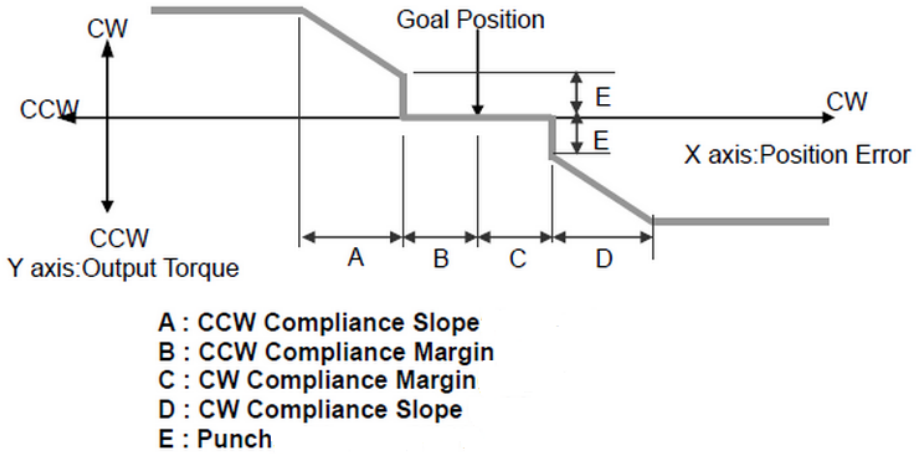

Figure 3.18: Controller of the Servo Motor

Figure 3.18 demonstrates the relationship between output torque and position of these servo motors. There are two terms to regulate the motor controller: compliance margin and compliance slope. Compliance margin represents the error between goal position and present position and assumes a value in 0–255 range. The more this margin increases, the more difference occurs. Compliance slope adjusts the level of torque near the goal position and can be set at 7 levels. The higher the compliance slope, the more compliance can be achieved [26]. Figures 3.19, 3.20 and 3.21 present real-time control results for the first joint q_6 of the wrist.

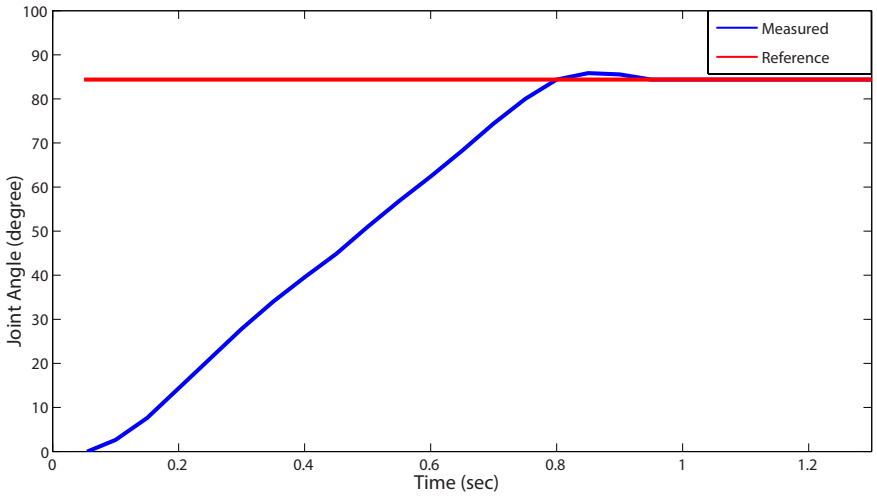

Figure 3.19: System Response under Unit Step Input

Figure 3.19 illustrates the regulation performance of the servo motor controller when 90 degrees unit step is commanded.

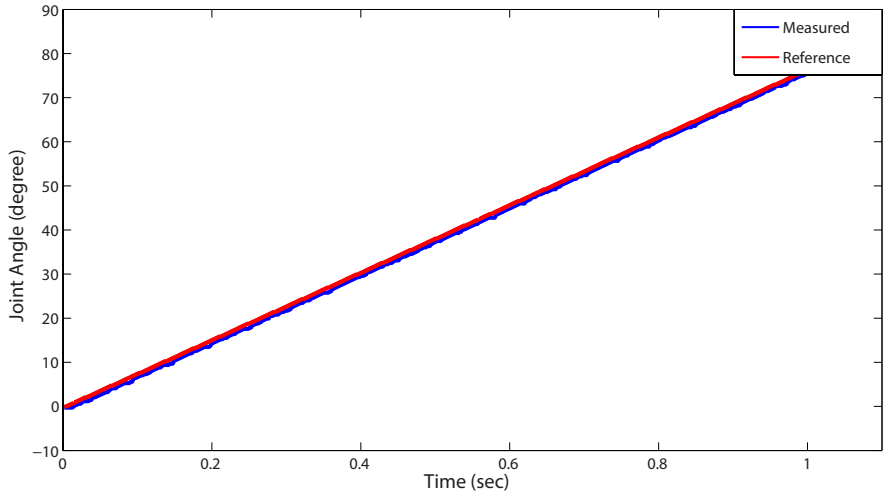

Figure 3.20: System Response under Ramp Input

Figure 3.20 shows the system response when a ramp input is applied.

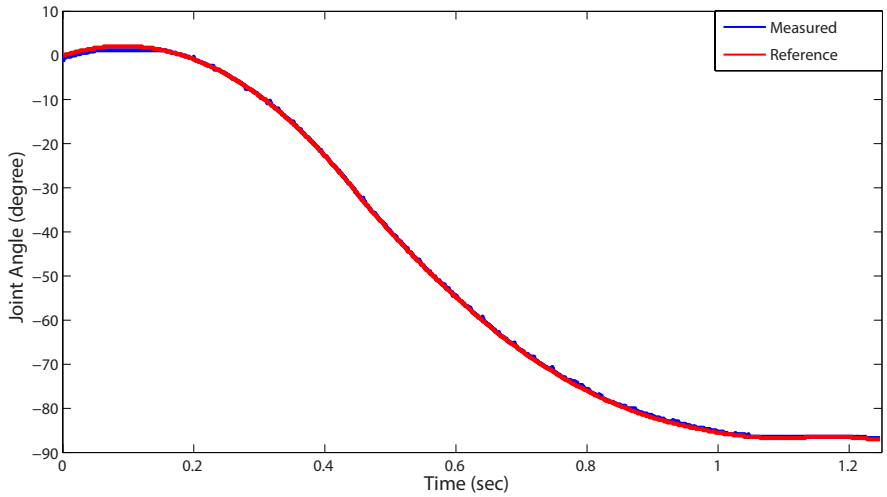

Figure 3.21: Trajectory Tracking Performance of the Wrist Joints

Figure 3.21 depicts the system behavior when a joint trajectory generated by a motion planner is commanded.

3.4 Kinematic Model of the Holonomic Base

This section presents the inverse kinematics of the 8 DoF redundant holonomic base. The inverse kinematics solution enables joint space control of the base when a collision-free navigation plan is provided by the motion planner. The derivations in this section closely follow [27].

Holonomic base of CoCoA is equipped with four independently steered and driven wheels W_i, which are modeled as vertical discs that roll around their horizontal axles and rotate around a vertical axis that is passing through their center. The wheels are located at points P_i and their orientations are represented by q_i with respect to the base. In addition, the holonomic base is rotated with an amount of θ with respect to the Newtonian reference frame N. Each wheel is characterized by two velocities: linear velocity v_{W_i} and steering velocity V_{q_i}. We assume that there is not slip and each wheel satisfies rolling constraints. To avoid singularities in the kinematic solution when wheels become parallel, instantaneous center of rotation (ICR) is defined by a geometric path $\xi(t)$ that is followed by the holonomic base, rather being defined at the intersection of the axes of the wheels. If the desired path is known, then the curvature of this path can be calculated easily and used to solve for $\dot{\theta}$. Given $\dot{x}$ and $\dot{y}$

$$V = \sqrt{\dot{x}^2 + \dot{y}^2} \tag{3.1}$$

where V is the velocity of the base in N. Define

$$R = \sqrt{(g_x)^2 + (g_y)^2} \tag{3.2}$$

where g_x and g_y are the x and y components of the curvature. g_z component

is not considered, since holonomic base is constrained to move on the surface. Then, $\dot{\theta}$ can be calculated as

$$\dot{\theta} = \frac{V}{R} \tag{3.3}$$

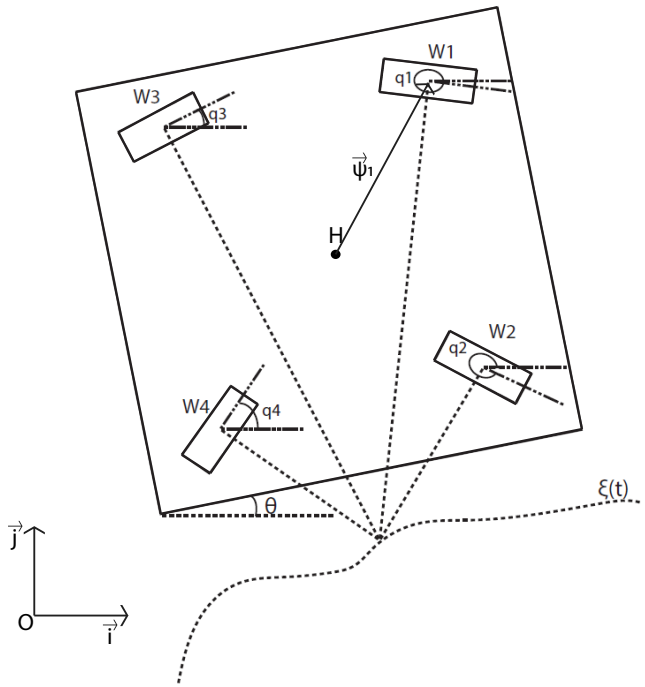

Figure 3.22: Schematic diagram of the holonomic platform equipped with four steered and driven wheels

Define the center point of each wheel to have the coordinates P_{i_x}, P_{i_y} and P_{i_z}, where $i = 1, 2, 3, 4$. Also let $\vec{\psi_i}$ be the vector that is defined between the center of the base and the wheels. Velocities at the center of wheels can be calculated as

$$\vec{V_{W_i}} = \dot{x}\vec{\imath} + \dot{y}\vec{j} + \dot{\theta}\vec{k} \times \vec{\psi_i} \tag{3.4}$$

Assumption of rolling without slipping implies that

$$-\sin(\theta + q_i)\dot{x}_i + \cos(\theta + q_i)\dot{y}_i \tag{3.5}$$

where

$$\begin{bmatrix} x_i \\ y_i \end{bmatrix} = \begin{bmatrix} x \\ y \end{bmatrix} + R(\theta)P_i \tag{3.6}$$

Combining Equations (5) and (6), non-holonomic constraints equations can be derived as

$$\begin{bmatrix} -\sin(\theta+q_1) & \cos(\theta+q_1) & \triangle_1 & 0 & \cdots & 0 \\ -\sin(\theta+q_2) & \cos(\theta+q_2) & \triangle_2 & 0 & \cdots & 0 \\ -\sin(\theta+q_3) & \cos(\theta+q_3) & \triangle_3 & 0 & \cdots & 0 \\ -\sin(\theta+q_4) & \cos(\theta+q_4) & \triangle_4 & 0 & \cdots & 0 \end{bmatrix} \begin{bmatrix} \dot{x} \\ \dot{y} \\ \dot{\theta} \\ \dot{q_1} \\ \dot{q_2} \\ \dot{q_3} \\ \dot{q_4} \end{bmatrix} = 0 \tag{3.7}$$

where $\triangle_i = P_{x_i}\cos(q_i) + P_{y_i}\sin(q_i)$. To compute q_i, i^{th} constraint in Equation (3.7) should be solved for q_i. Solving for only two of the q_i using this equation is enough to calculate all other q_i.

$$q_i = arctan2\ \frac{-\sin(\theta)\dot{x} + \cos(\theta)\dot{y} + P_{i_x}\dot{\theta}}{\cos(\theta)\dot{x} + \sin(\theta)\dot{y} + P_{i_y}\dot{\theta}} \tag{3.8}$$

Moreover, since there is not slip, the angular velocity $\dot{\alpha}_i$ of each wheels can be found by simply dividing the linear velocity of the wheel by its radius:

$$\dot{\alpha}_i = \frac{\mid V_{W_i} \mid}{r} \tag{3.9}$$

3.5 Passive Velocity Field Control of the Holonomic Base

Passive Velocity Field Control (PVFC) has two distinct features that differentiate it from other control schemes. Firstly, instead of defining the task as a trajectory tracking problem, to define the desired behavior PVFC uses velocity fields defined on the configuration manifold of the system. Hence, PVFC ensures tracking of a desired contour, while timing of the task is dictated by the amount of energy in the system. Secondly, PVFC renders the mechanical system under closed-loop control into energetically passive system with respect to external forces. This ensures the safety of this control approach. In particular, PVFC is developed for robotic applications that require close interaction between the robot and humans or other objects that are likely to be damaged by the robot [28].

PVFC decouples the task to be performed from the speed of the task. Basically, the task is expressed as a predefined velocity field, while the speed of the system is adjusted by instantaneous energy of the closed loop system.

To implement PVFC, firstly a velocity field should be generated by defining a reference velocity at each point in the manipulator's task space. To define the velocity field, we have used the online velocity field generation method proposed for parametric curves [29]. This approach relies on a feedback stabilized tracking algorithm to identify the closest point on the desired contour to the holonomic base. Once the closest point on the desired contour is calculated, tangential vector field $V^{\parallel}$ and normal vector field $V^{\perp}$ can easily

be constructed as follows:

$$V^{\parallel} = v\,\mathbf{f_s}(s^*) \tag{3.10}$$

$$V^{\perp} = \chi\,(\mathbf{r}^{EE} - \mathbf{f}(s^*)) \tag{3.11}$$

where $\mathbf{r}^{EE}$ symbolizes the position of the center of the holonomic base, and v and χ are scaling parameters. The closest point on the parametric curve $\mathbf{f}(s)$ is denoted by the symbol s^*, while the unit tangent vector at s^* is represented by $\mathbf{f_s}(s^*)$.

By simple superposition of these two vector fields, the desired velocity field can be constructed as indicated in Figure 3.23. The online method does not necessitate calculation of velocity field for all possible configurations of the holonomic base since velocity field is generated online for each actual position. The rest of the presentation closely follows [30–33].

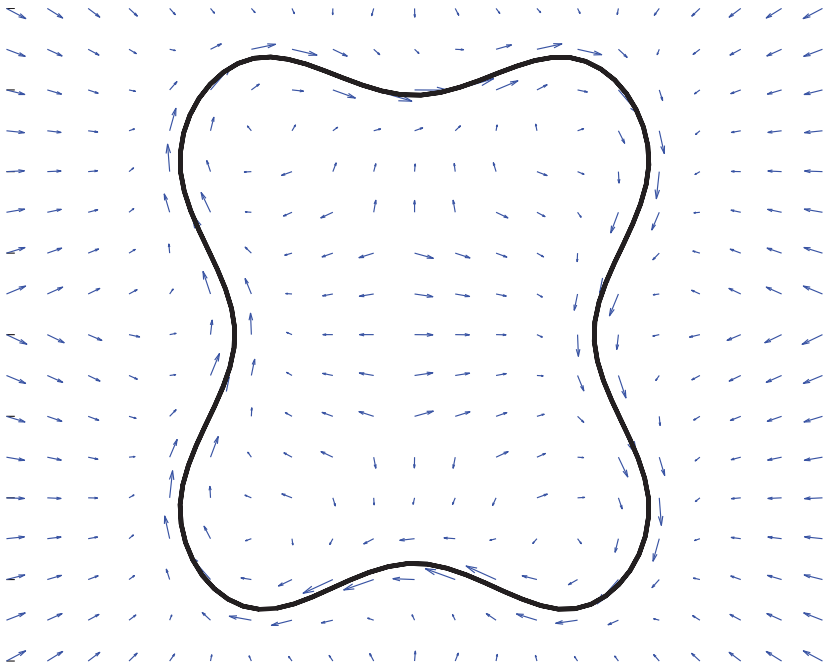

Figure 3.23: Desired Velocity Field

Define the dynamics of the holonomic base as follows

$$\mathrm{M}(\mathrm{q})\ddot{\mathrm{q}} + \mathrm{C}(\mathrm{q}, \dot{\mathrm{q}})\dot{\mathrm{q}} = \tau + \tau_{\mathrm{e}} \tag{3.12}$$

where $\mathrm{M}(\mathrm{q}) \in \mathbb{R}^{n \times n}$ is the inertia matrix, $\mathrm{C}(\mathrm{q}, \dot{\mathrm{q}}) \in \mathbb{R}^{n \times n}$ is the Coriolis matrix and joint positions are denoted as q. τ represents control forces, while external forces are represented as τ_{e}. PVFC ensures passivity of the system with respect to external force inputs τ_{e} implying

$$\int_0^t {\tau_{\mathrm{e}}}^T \dot{\mathrm{q}}\, d\tau \geq -c^2 \tag{3.13}$$

where c is some real number. PVFC regulates the contour error to zero, while the velocity of the system approaches to a scaled multiple of the velocity dictated by the velocity field. For any initial condition $(\mathrm{q}(0), \dot{\mathrm{q}}(0))$, the controller guarantees that there exist a constant $\rho > 0$ such that

$$\lim_{t \to \infty} \dot{\mathrm{q}}(t) - \rho \mathrm{V}(\mathrm{q}(t)) = 0. \tag{3.14}$$

when $\tau_{\mathrm{e}} = 0$. Adjusting the initial energy of the system, or supplying energy through work done on the system, or tuning the instantaneous energy of the system through extra controller terms, one can determine the speed of the task.

To fulfill control specifications that are represented in Eqnuations (3.13) and (3.14), dynamics of a fictitious flywheel is augmented to the system. The original system and a fictitious flywheel with a mass M_F form the augmented system. Here, the fictitious flywheel plays the role of an extra energy storage element. The kinetic energy of the augmented system can be expressed as

$$\bar{k}(\bar{\mathrm{q}}, \dot{\bar{\mathrm{q}}}) = \frac{1}{2} \dot{\bar{\mathrm{q}}}^T \bar{\mathrm{M}}(\bar{\mathrm{q}}) \dot{\bar{\mathrm{q}}} \tag{3.15}$$

where inertia matrix of the augmented system is represented as $\bar{\mathrm{M}}$ and the augmented configurations and velocities are denoted by $\bar{q}$ and $\dot{\bar{q}}$, respectively. To acquire a positive and constant kinetic energy for the augmented system $\bar{k}(\bar{\mathrm{q}}, \bar{\mathrm{V}}(\bar{\mathrm{q}}))$, velocity of the flywheel $V_{n+1}(\mathrm{q})$ is calculated as

$$V_{n+1}(\mathrm{q}) = \sqrt{\frac{2}{M_F}\left(\bar{E} - \frac{1}{2}\mathrm{V(q)}^T\mathrm{M(q)V(q)}\right)} \tag{3.16}$$

$$\bar{k}(\bar{\mathrm{q}}, \bar{\mathrm{V}}(\bar{\mathrm{q}})) = \frac{1}{2}\bar{\mathrm{V}}(\bar{\mathrm{q}})^T\bar{\mathrm{M}}(\bar{\mathrm{q}})\bar{\mathrm{V}}(\bar{\mathrm{q}}) = \bar{E} > 0 \tag{3.17}$$

Then, the augmented desired velocity field $\bar{\mathrm{V}}(\bar{\mathrm{q}})$ can be formed as

$$\bar{\mathrm{V}}(\bar{\mathrm{q}}) = \left[\mathrm{V(q)}^T, V_{n+1}(\mathrm{q})\right]^T \tag{3.18}$$

The energy of the augmented system $\bar{E}$ has to be chosen adequately large enough to ensure real solutions for Equation (3.16). By using a feed-forward term $\bar{\tau}_{\mathrm{c}}$ for dynamic compensation and a feedback term $\bar{\tau}_{\mathrm{f}}$ to compensate for the contour error, a skew-symmetric control law is implemented as

$$\bar{\tau}(\bar{\mathrm{q}}, \dot{\bar{\mathrm{q}}}) = \bar{\tau}_{\mathrm{c}}(\bar{\mathrm{q}}, \dot{\bar{\mathrm{q}}}) + \bar{\tau}_{\mathrm{f}}(\bar{\mathrm{q}}, \dot{\bar{\mathrm{q}}}) \tag{3.19}$$

with

$$\bar{\tau}_{\mathrm{c}} = \underbrace{\frac{1}{2\bar{E}}(\bar{\mathrm{w}}\bar{\mathrm{P}}^{\mathrm{T}} - \bar{\mathrm{P}}\bar{\mathrm{w}}^{\mathrm{T}})}_{\text{skew symmetric}}\dot{\bar{\mathrm{q}}} \tag{3.20}$$

$$\bar{\tau}_{\mathrm{f}} = \gamma\underbrace{(\bar{\mathrm{P}}\bar{\mathrm{p}}^{\mathrm{T}} - \bar{\mathrm{p}}\bar{\mathrm{P}}^{\mathrm{T}})}_{\text{skew symmetric}}\dot{\bar{\mathrm{q}}} \tag{3.21}$$

where convergence rate is determined by a control gain $\gamma \in \mathbb{R}$ in Equation (3.21), which is not necessarily positive. The momentum of the augmented system and desired momentum are denoted by the terms $\bar{p}$ and $\bar{P}$, respectively. The inverse dynamics necessary to follow the desired velocity field is denoted by $\bar{w}$. Mathematically,

$$\bar{\mathrm{p}}(\bar{\mathrm{q}}, \dot{\bar{\mathrm{q}}}) = \bar{\mathrm{M}}(\bar{\mathrm{q}})\dot{\bar{\mathrm{q}}} \tag{3.22}$$

$$\bar{\mathrm{P}}(\bar{\mathrm{q}}) = \bar{\mathrm{M}}(\bar{\mathrm{q}})\bar{\mathrm{V}}(\bar{\mathrm{q}}) \tag{3.23}$$

$$\bar{\mathrm{w}}(\bar{\mathrm{q}}, \dot{\bar{\mathrm{q}}}) = \bar{\mathrm{M}}(\bar{\mathrm{q}})\dot{\bar{\mathrm{V}}}(\bar{\mathrm{q}}) + \bar{\mathrm{C}}(\bar{\mathrm{q}}, \dot{\bar{\mathrm{q}}})\bar{\mathrm{V}}(\bar{\mathrm{q}}) \tag{3.24}$$

where the i^{th} component of $\dot{\bar{\mathrm{V}}}$ is calculated as

$$\dot{\bar{V}}_i(\bar{\mathrm{q}}) = \sum_{k=1}^{n+1} \frac{\partial \bar{V}_i(\bar{\mathrm{q}})}{\partial \bar{q}_k} \dot{\bar{q}}_k. \tag{3.25}$$

Figures 3.24–3.29 illustrate simulation results of the holonomic base under PVFC while performing a contour tracking task. Figure 3.24 shows the reference contour to be followed and path followed by the holonomic base of CoCoA.

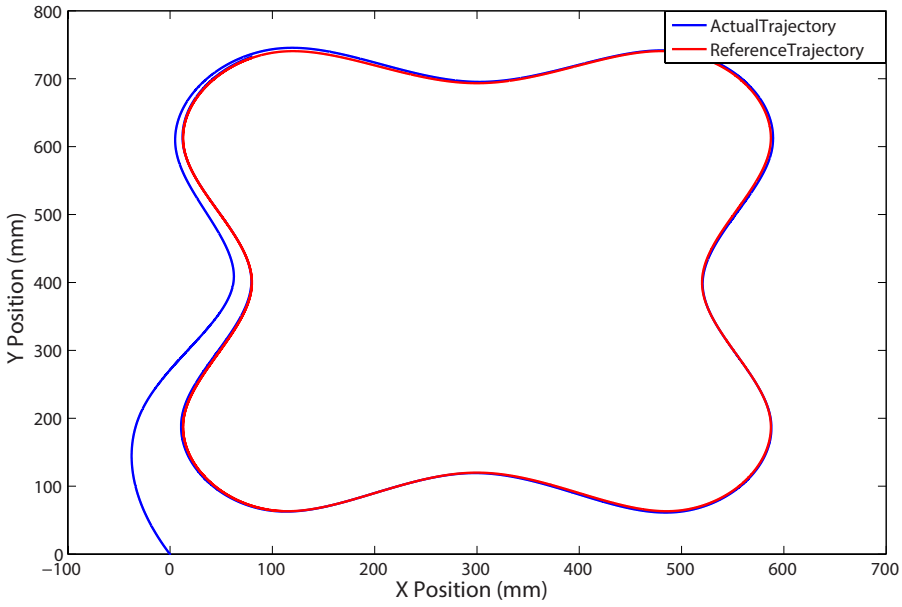

Figure 3.24: Reference Contour and Path Traced by the Holonomic Base

Figure 3.25 presents the configuration of the holonomic base on the contour at different time instances. We have used Matlab Virtual Reality toolbox to capture these snapshots.

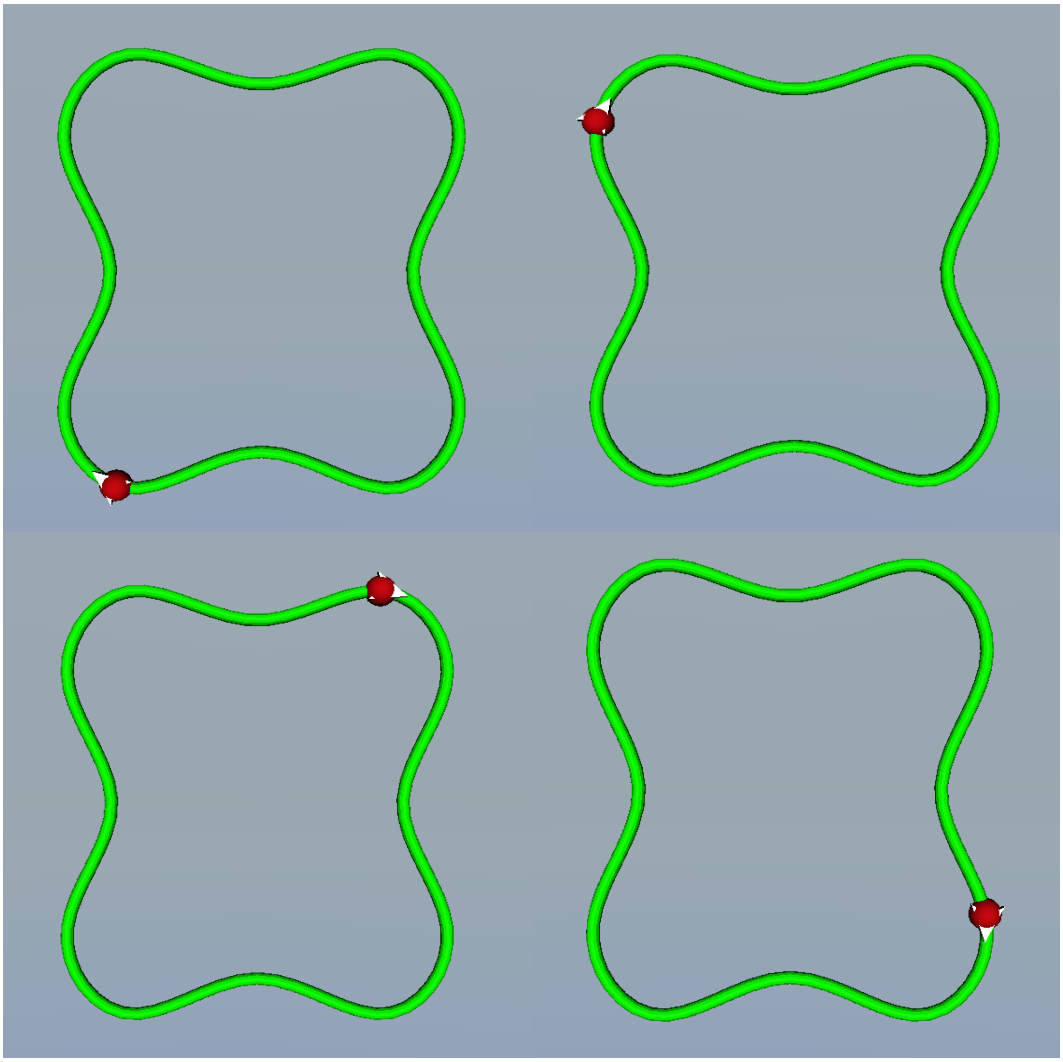

Figure 3.25: Different Configurations of the Holonomic Base on the Contour

Figures 3.26–3.29 presents contour tracking performance and contour error along x and y directions, respectively.

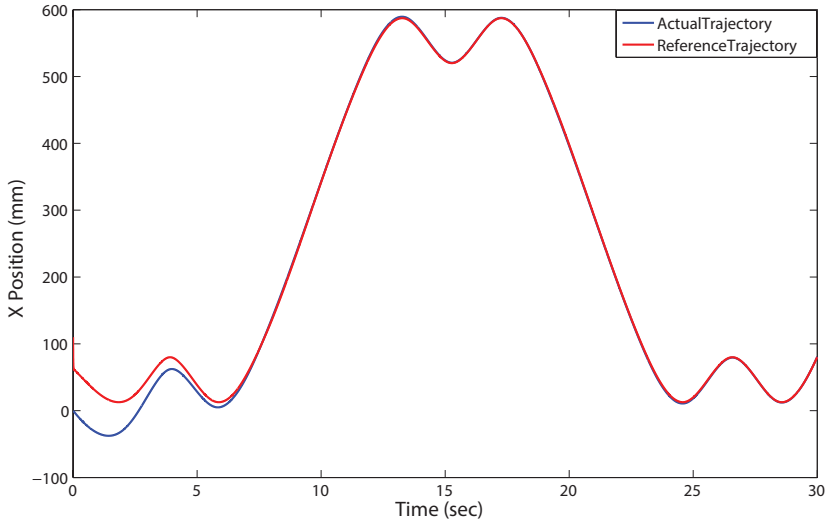

Figure 3.26: Reference and Actual Positions along x Direction

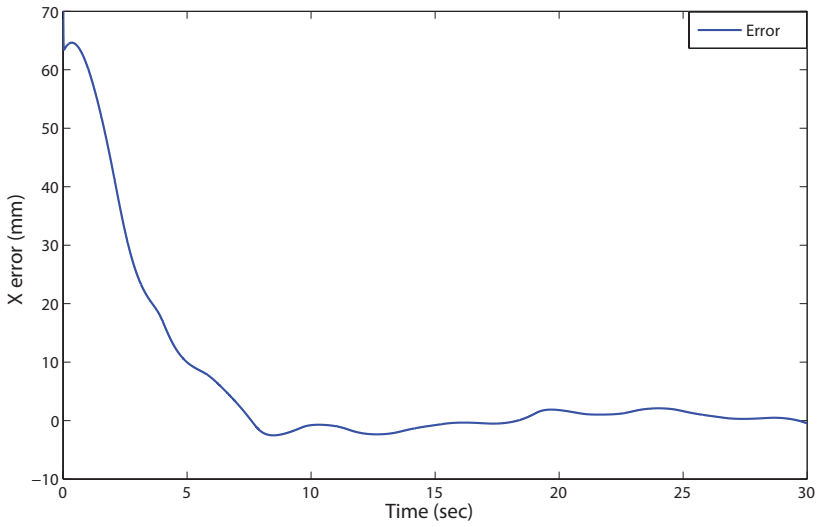

Figure 3.27: Contour Error along x Direction

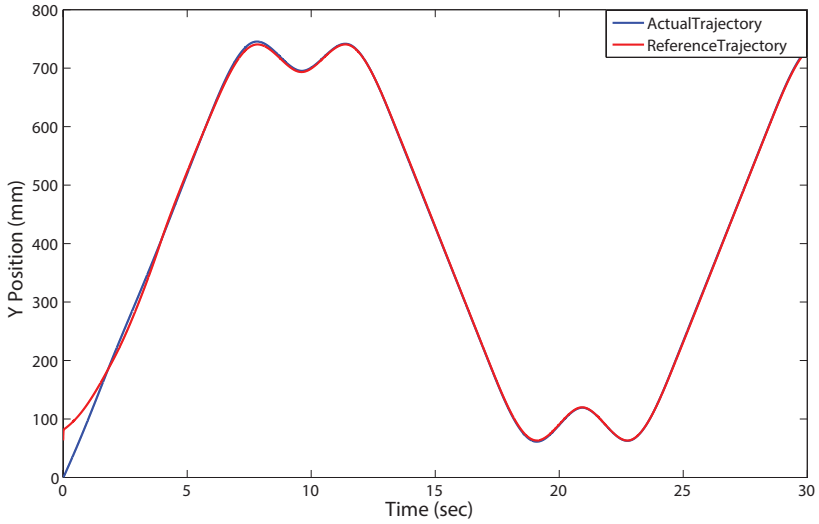

Figure 3.28: Reference and Actual Positions along y Direction

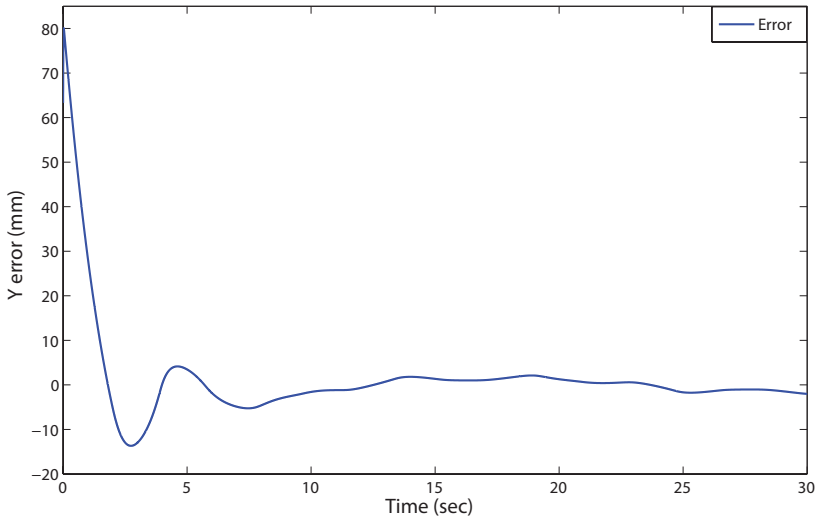

Figure 3.29: Contour Error along y Direction

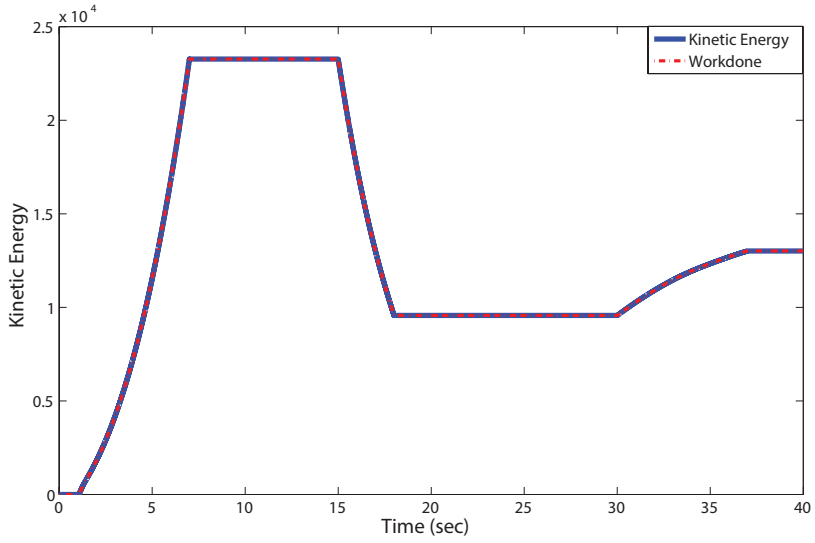

Figure 3.30: Kinetic Energy of Augmented System

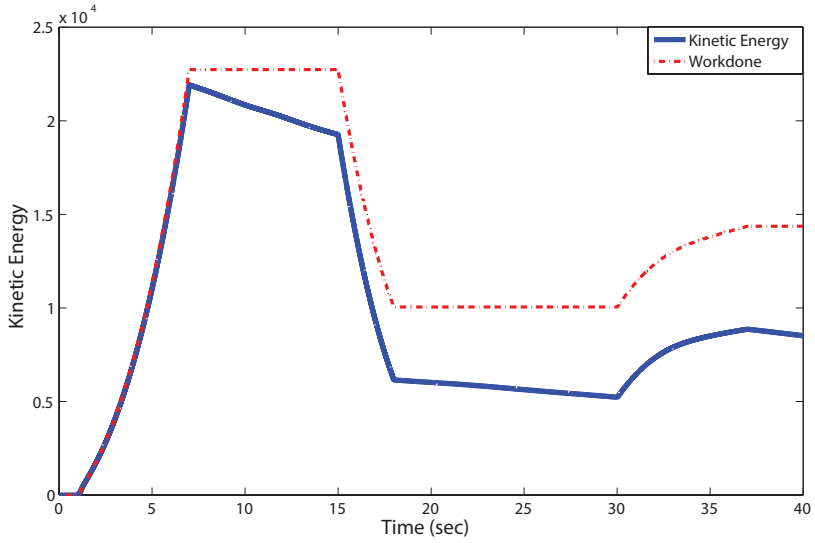

Figure 3.31: Kinetic Energy of Augmented System Under Damping Effect

Figures 3.30 and 3.31 illustrate the passivity of the system with respect to external forces. In particular, these plots persent kinematic energy of the

system, when damping is negligible and available in the system., respectively. In these simulations, firstly, tangential force along the trajectory is applied during 1–7 sec and the kinetic energy of the system increases as much as this positive work done by the system (minus losses due to damping in Figure 3.31). No force is applied to the system during 7–10 sec and kinetic energy stays constant when there is no dissipation term. During 15–17 sec, a negative tangential force along the trajectory is applied and the kinetic energy of the system decreases as much as this negative work done by the system (plus the losses due to damping in Figure 3.31). No force is applied to the system during 17–30 sec and kinetic energy stays constant when there is no dissipation term. Finally, a normal force is applied during 30–36 sec, and kinetic energy of the system increases as much as the work done by this normal force. Note that a contour error forms when normal forces are exerted on the system and the velocity of the robot does have a normal component to the contour, which results in the positive work done by such forces. It is important to emphasize that throughout the simulations, the closed loop system is completely passive with respect to external forces and the controller does not add (or extract) energy from the system, but simply stores/releases energy in its fictions flywheel. The only change in the kinetic energy of the system is due to work done by the external forces: hence, the passivity of the system with respect to external forces is ensured.

3.6 Discussion

Joint space control is implemented on hardware for both arms and wrists. Joint trajectories for the arms and wrists are generated by a motion planner explained in the next chapter. Navigation plan detailing the contour to

be traced by the center of mass of the holonomic base is also generated by these motion planners. Given such collision-free contours in parametric form, PVFC can be used to track these contours and can do so while ensuring passivity of the system with respect to external forces. Note that this passivity aspect is important, since it enables safe physical interaction between the robot and human users.

Physical implementation of PVFC could not be completed due to several hardware problems that could not be resolved by the writing of this thesis.

Chapter IV

4 Software Integration of CoCoA Service Robot

For motion/navigation/grap planning and dynamic simulation of CoCoA, Open Robotics and Animation Virtual Environment (OpenRAVE) is used. Use of this software allows us to develop, compute, test, and deploy motion plans to the hardware controllers of CoCoA for real-world robotics applications. OpenRAVE is selected as a software integration environment since it excels at analysis of geometric and kinematic data at high rates. It provides an easy to use dynamic simulation interface and allows for custom code to be integrated through Python programming. In particular, many command-line tools are available through OpenRAVE to enable easy integration of robots and utilization of its large repertoire of planners. Furthermore, OpenRAVE features a small run-time core that allows the software to be used inside controllers and/or larger frameworks [34].

4.1 Robot Definition

XML file format is preferred to define geometric/kinematic/dynamic properties of CoCoA for software integration. Many robotics software middleware, including ROS and OpenRave supported robot definitions in XML format. The XML format is modular as it allows association of different XML files in a single file. In this way, each robot module as well as the

manipulated objects and environment can be defined in separate files and merged together. Moreover, XML supports importing robot/objects models from VRML or IV files. There are various XML files that have been created for defining CoCoA and test environments in software:

- **Environment** – can include multiple robots and objects. It also allows for specification of camera pose or background color.
- **KinBody** – Kinbodies are basic objects that form all other objects or robots. Basically, a kinematic body is composed of series of kinbodies and joints which connect those kinbodies.
- **Robot** – OpenRAVE needs at least one kinbody to form a robot. Robots may also include **Manipulators** or **AttachedSensors** that are used to specify robot's manipulation and sensing capabilities.

To form CoCoA's XML definition, VRML models of each are used. These files include all the material and geometric properties of the corresponding links. Joint limits and joint velocities are specified while connecting these links together to from the desired kinematic arrangements. Since XML format provides modularity, XML files for the each arm, wrist, gripper, torso and holonomic base are created separately. Then, all of these bodies are linked to each other with dummy fixed joints to form CoCoA with 25 DoF.

Following code illustrates a sample of XML file:

```
-<KinBody name="Right_Arm">
        -<Body name="Arm_Base" type="dynamic">
        <Translation>-0.2 -0.09 1.1</Translation>
                <RotationAxis>0 0 1 30</RotationAxis>
                -<Geom type="trimesh" modifiable="false">
                        <render>/home/wrl_file_location</render>
                        <data>/home/wrl_file_location</data>
                </Geom>
                -<Mass type="box">
                        <com>0 .005 0</com>
                        <total>0.25</total>
                </Mass>
        </Body>

        -<Body name="R_First_Link" type="dynamic">
                <offsetfrom>Arm_Base</offsetfrom>
                <Translation> 0.0 0.0 -0.15</Translation>
                <RotationAxis>1 0 0 -90</RotationAxis>
                -<Geom type="trimesh" modifiable="false">
                        <data>/home/wrl_file_location</data>
                        <render>/home/wrl_file_location</render>
                </Geom>
                -<Mass type="box">
                        <total>.2</total>
                </Mass>
        </Body>

        -<Joint name="R_First_Joint" type="hinge" circular="true">
                <Body>Arm_Base</Body>
                <Body>R_First_Link</Body>
                <offsetfrom>R_First_Link</offsetfrom>
                <axis> 0 1 0 </axis>
                <limitsdeg>-180 180</limitsdeg>
                <limitsvel>-3 3</limitsvel>\
                <resolution>1</resolution>
        </Joint>
```

Figure 4.1: Sample XML Code

4.2 Inverse Kinematics Database

We utilize IKFast module [35] of the OpenRAVE to analytically solve for the inverse kinematics equations of each arm. Given an XML manipulator model, IKFast generates optimized C++ files that can be used for simulations. In particular, as long as possible, IKFast utilizes closed-form analytical solutions and this aspect is crucial because of two main reasons:

- Closed form inverse kinematic solutions are much faster than solutions that rely on numerical iteration. To compute feasible motion plans, planners need to process thousands of configurations per second. Solutions on the order of **4 microseconds** can be achieved by the closed-form code generated by IKFast. On the other hand, most numerical solutions are on the order of 10 milliseconds, if good convergence is obtained.

- The null space of the solution set can be examined, because all solutions can be calculated.

Inverse kinematic solutions are required in order to place the end-effector coordinate system of the robot in the world, while maintaining joint limits and user-defined constraints. We have used different IK Types of IKFast module to match the task constraints. Each of these IK types feature their own advantages. The IK types utilized in this work are

- **Transform6D** – end-effector frame reaches desired 6D configuration

- **Rotation3D** – end-effector frame reaches desired 3D rotation

- **Translation3D** – origin of the end-effector frame reaches the desired 3D translation

Moreover, IKFast can be used with any number of joints arranged in a serial kinematic chain. If the serial kinematic chain is redundant, that is, has more DoF than IKType requires, then the user is expected to set the redundant joints as *freejoint* such that the number of unknown joints matches the DoF of the IK type. Defining freejoints may decrease workspace of the manipulator; when a joint is defined as freejoint, its value is changed incrementally and this approach does not consider the values between two increments. Therefore, workspace of the manipulator slightly decreases; however, IKFast provides closed-form solutions that significantly speed up calculations and allow for different freejoint configurations to be tested in a short amount of time. Therefore, the workspace loss is negligible for many cases.

CoCoA's arms are redundant for Transform6D, since each arm features 7 DOFs. We set the first joint as a freejoint to get a closed-form solution, thanks to the spherical wrist. Using IKFast for inverse kinematics of CoCoA provides following advantages;

- All possible inverse kinematic solutions (up to 16 for serial robots) are calculated.
- Analytical closed form solutions are found when the wrist axes are designed to be intersecting.
- Degenerate cases where 2 or more axes align and cause infinite solutions are automatically detected.
- Invalid solutions are detected by checking if square roots are given negative values or arc sines and arc cosines are given inputs exceeding the feasible [-1,1] range.

- All divide by zero conditions are automatically checked and handled.
- Generated C++ code is **independent** of OpenRAVE or any other library; hence, can be used for real-time controls.
- If the robot is redesigned, serial configuration of the robot can be arbitrary set, for instance, by adding a wrist with non-intersecting axes.

Furthermore, OpenRAVE's inverse kinematic module allows us to integrate following feasibility checks into inverse kinematics calculations [35]:

- **Environment Collisions** – to check whether IK solutions collide with the environment or not,
- **Self Collisions** – to check whether robot collides with itself or not,
- **Joint Limits** – to check whether pre-defined joint limits are violated or not,

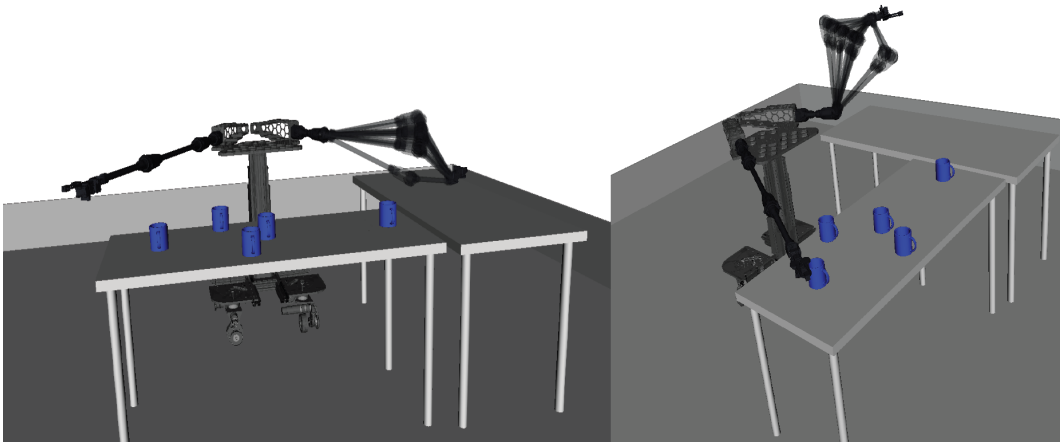

Figure 4.2: Possible Inverse Kinematic Solutions for Various Targets

Figure 4.2 depicts several inverse kinematic solutions that are generated by IKFast for each target point. The inverse kinematics performance for CoCoA arms has been characterized by IKTest option of IKFast: success rate is 98.9%, incorrect solution rate is 0.0% and no solution are is 1% and missing solution rate is 0.6%.

4.3 Defining and Generating the Grasp Database

Grasp database contains all possible force closure valid grasps for a specific gripper and a specific object. Content of the database can be used during grasp planning procedure to determine kinematically-feasible collision-free trajectories. To compute feasible grasp configurations and to reach these configurations through motion plans, we have used the grasping module of OpenRAVE. This module can be used with robot end-effector and objects pairs to simulate grasps and to evaluate quality of these grasps. Once feasible grasps with good characteristics are identified and cached, these grasps can be used for more complex grasp planning applications. In particular, a grasp can be simulated by providing an initial pose and initial joint angles (preshape) to the end-effector. Consequently, the end-effector starts to move along a direction that is generally along the normal of the palm, until the end-effector makes contact with the target object. Once the end-effector touches the target object, fingers of the gripper gradually close around the object until they cannot be closed any further.

To find out feasible approach directions, grasp set creation process uniformly samples the surface of the target object. However, uniform sampling of the actual geometric surface may give rise to undesirable results due to possible non-convexities on the surface, such as the handle of a cup. Instead

of using the surface of the target object for sampling, the bounding box of the target object can be used to result in a simpler, more efficient and more robust approach. Figure 4.3 illustrates sampling of bounding box for an object.

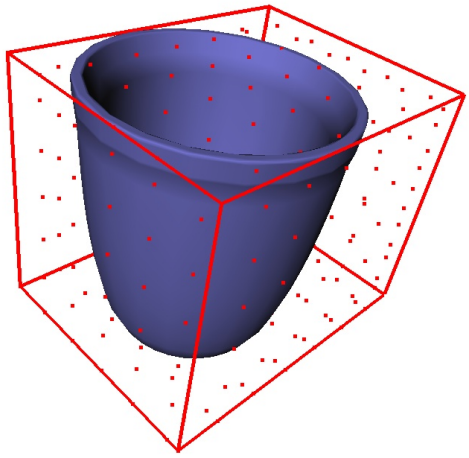

Figure 4.3: Sampling of the Bounding Box

Uniformly sampled points on the surface of the bounding box are used as starting points of rays that trace inwards and intersect with the surface of the object. The normal vectors of the object's surface at those intersection points are used as possible approach directions to grasp the object. The red lines in Figure 4.4 depicts possible approach directions for that specific object.

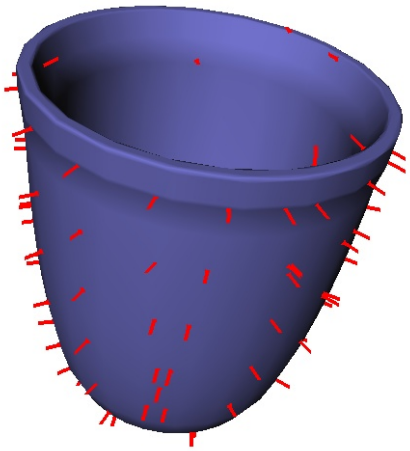

Figure 4.4: Possible Approach Directions

As soon as the initial pose of the gripper, preshape, and approach direction are chosen, the grasp planner module examines the contact points of the grasp and checks them for force closure. Grasper planner also features several advantages: it allows for specification of grasp parameters (roll, direction, and center offset, etc.) in the target body frame and robot transformations are performed by the grasper planner according to these defined grasp parameters [36]. Figure 4.5 presents several feasible grasps by CoCoA.

Figure 4.5: Samples of Feasible Grasps Performed by CoCoA

4.4 Defining and Generating the Kinematic Reachability and Inverse Reachability Databases

Kinematic reachability database contains IK solutions as quaternians and translation coordinates as well as number and density of these IK solutions for each point in the space. Basically, kinematic reachability database defines the workspace of a manipulator. It is generated by preprocessing the reachable volume and caching this information as a look-up date. This preprocessing stage is computationally intensive, but needs to be performed only once for each manipulator. The reachability database is useful since it significantly speeds up real-time retrieval of this information.

Kinematic reachability database is generated separately for each manipulator of the robot, if the manipulators have different kinematic chains. However, since CoCoA has two identical arms, gerenating the database only for one arm is sufficient. Generating the kinematic reachability database for CoCoA takes around 12 hours in a standard PC workstation (Intel Core i5 3210M @ 2.5 GHz with 4 G of memory).

Kinematic reachability database contains two important information: reachabilitystats and reachability. Reachabilitystats is $N \times 8$ array of all poses that are reachable. The first 7 columns contain the quaternions and translation coordinates, while the last column signifies the number of IK solution present at that configuration. Reachability is a $K \times K \times K$ voxelized map that represents the density of solutions for each point. The higher this density, the more rotations of the arm can be solved for [37]. Kinematic reachability module can be used to check whether an object is kinematically reachable or not, while simultaneously checking for collisions with the environment.

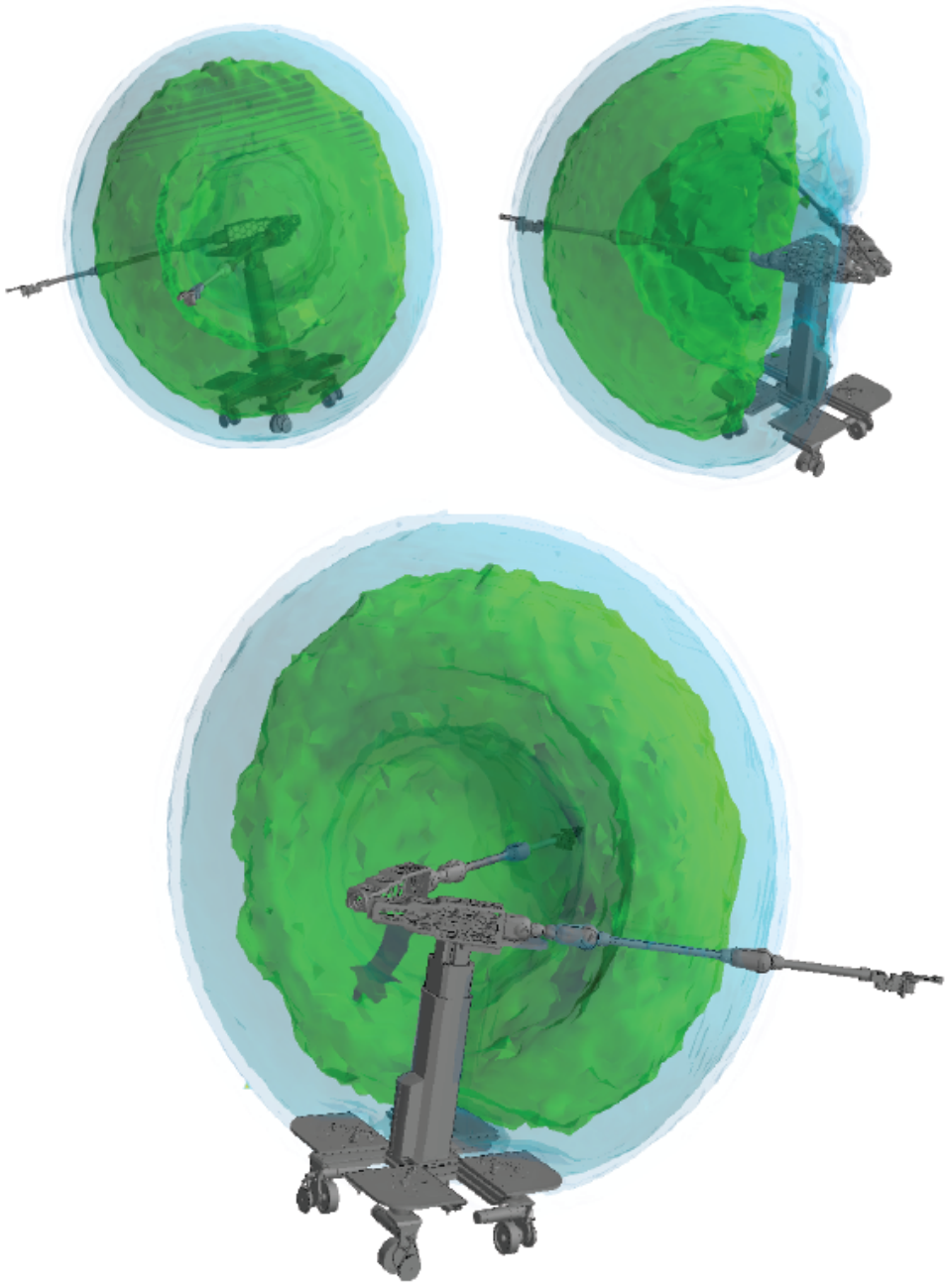

Figure 4.6: Kinematic Reachability of the Left Arm of CoCoA

Figure 4.6 depicts workspace of the left arm of CoCoA, where colors indicate densities.

Inverse reachability module is another useful tool that is utilized to compute and store feasible configurations of the robot base such that the robot can perform a specific grasp [38]. Inverse reachability module uses the reachability space to sample for base locations and caches feasibility of such reaches for later use.

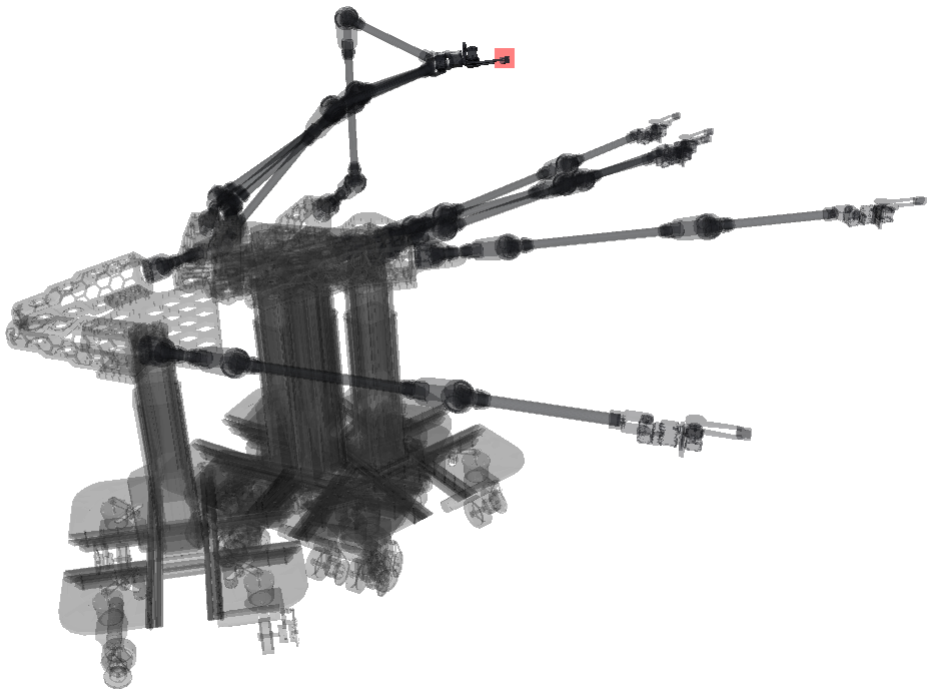

Figure 4.7: Possible Base Positions to Perform a Specific Manipulation

In Figure 4.7 five different base locations for the left arm of CoCoA to achieve a grasp of the target are illustrated. The red square represents the target.

4.5 Navigation Planning

We use navigation planners based on Rapidly-exploring Random Trees (RRT) [39]. Since CoCoA is planned to operate in dynamic environments, single query RRTs are preferred. Moreover, a variant of RRT, the RRT* algorithm, is asymptotically optimal that means solution converges to optimal solution by time. RRT can swiftly search high dimensional spaces that contain both algebraic constraints (caused by obstacles) and differential constraints (caused by nonholonomic constraints and dynamics). RRT performs randomized search, where the key idea is to altering the exploration toward unexplored partition of the space by sampling points in the state space, and gradually pulling the search tree toward them. Algorithm 1 summarizes the underlying working principle of basic RRT.

Algorithm 1 RRT

initialization; T.add(q_{start})

while *iteration* $< K$ **do**

  q_{rand}=random configuration

  q_{near}=nearest neighbor in tree T to q_{rand}

  q_{new}=extend q_{near} toward q_{rand}

  if q_{new} *can connect to* q_{near} **then**

    T.addVertex(q_{new});

    T.addEdge(q_{near},q_{new});

  end

  if $\rho(q_{new}, q_{goal}) <$ *distanceToGoalTh* **then**

    break;

  end

end

Figure 4.8 illustrates navigation path of CoCoA from an initial point to a desired destination. In this example, the environment is designed to contain many obstacles to test the performance of navigation planner.

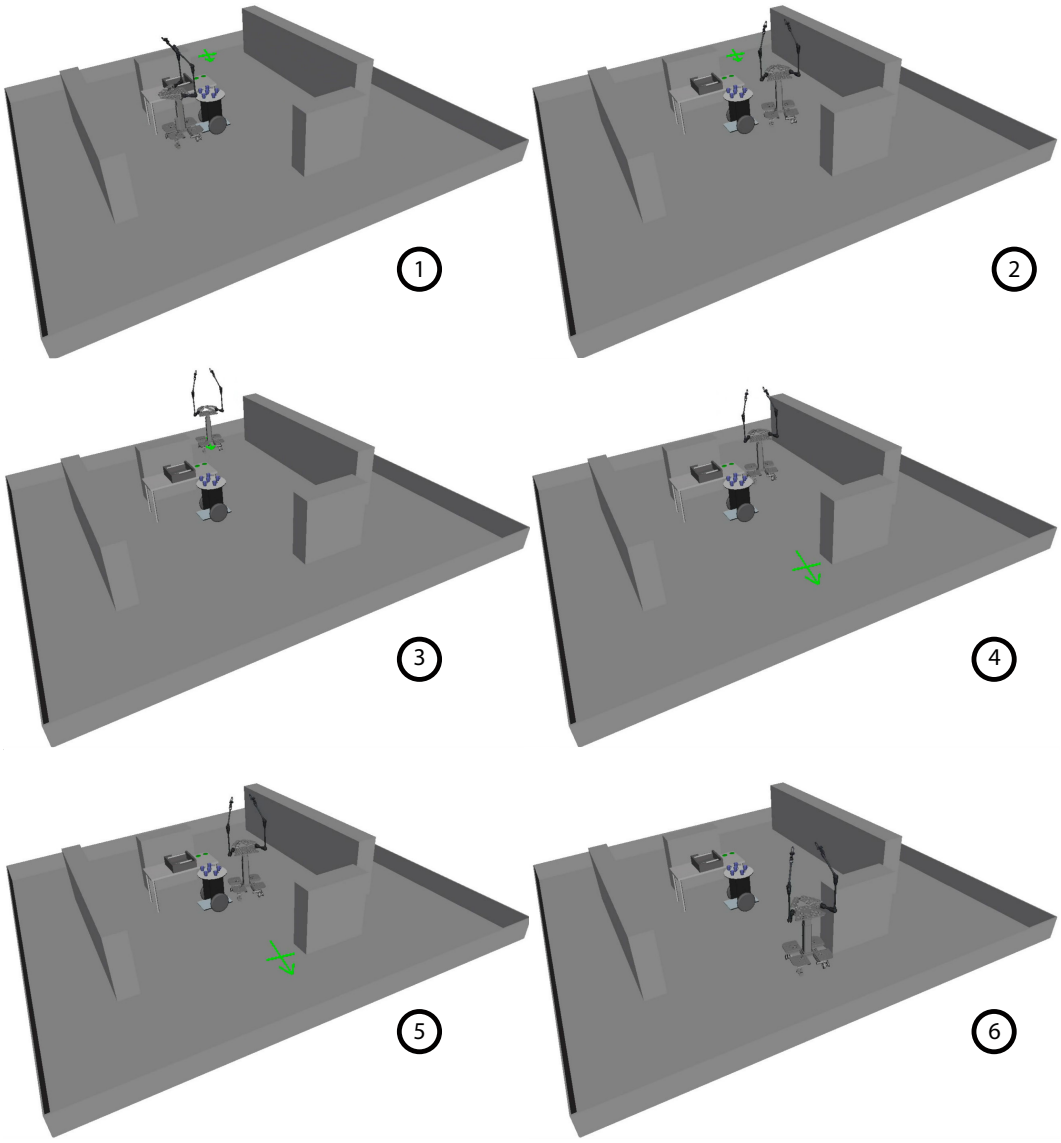

Figure 4.8: Navigation of CoCoA in an Environment with Obstacles

Chapter V

5 Case Studies using CoCoA Service Robot

This chapter presents several case studies that utilize CoCoA as a service robot. In particular, three dynamic simulations and a physical implementation are presented that illustrate several capabilities of the system.

5.1 Scenario 1: Reaching to a Shelf and Grasping an Object

In this scenario, CoCoA reaches to an object located at a high self and grasps an object lying on the self while the robot base is kept fixed. To execute the dynamic simulation of this scenario, first the grasp database is generated for the object end-effector pairs. Grasp database provides all feasible grasps that are collision-free and have a valid inverse kinematic solution. Once a valid grasp is selected, then the motion planner is called to calculate a feasible trajectory to grasp the object. Algorithm 2 presents the pseudocode used to execute this task.

Algorithm 2 Reaching to a Shelf and Grasping an Object

initialization; Generating inversekinematics and grasping databases

while *validgrasp != None* **do**

    if *IkSolution = True* **then**
        Grasp the object
    else
        Check for the next valid grasp
    end

end

abort manipulation

In Figure 5.1 Snapshot 1 CoCoA chooses a feasible grasp that is collision-free and has a valid inverse kinematic solution. In Snapshots 2-3, trajectories for each joints, that are generated by motion planners, are executed. Snapshot 4 illustrates that CoCoA can grasp the target object successfully.

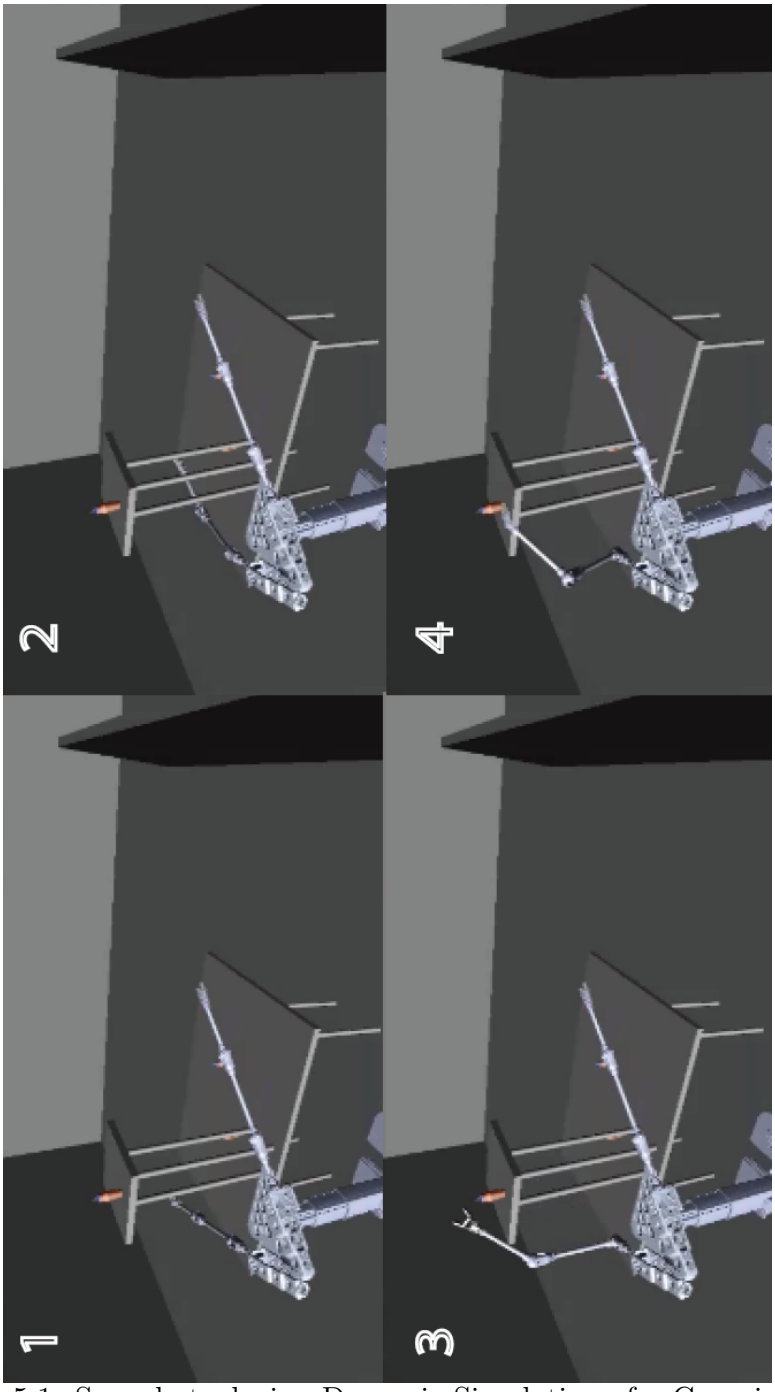

Figure 5.1: Snapshots during Dynamic Simulation of a Grasping Task

Figure 5.1 presents snapshots taken during dynamic simulation of the grasping task.

5.2 Scenario 2: Rearrangement of Objects on a Table

In this scenario, the goal is to tidy up 5 mugs randomly placed on a table. Location of the robot base is fixed: hence, the robot cannot adjust its base location to perform manipulations. In this scenario, the environment and task are more complex, since some of those mugs cannot be reached by the left arm of CoCoA. If this is the case, then the right arm of CoCoA should assist its left arm to fulfill the task. Therefore, while executing this scenario CoCoA should check which objects it can manipulate with which arm and act accordingly. If an object can be manipulated by the left arm, then CoCoA performs that manipulation right away. After all the objects that can be manipulated by the left hand are processed, CoCoA uses its right arm to fulfill the task if possible. If completion of the task is not feasible by right arm, then CoCoA places the object to an intermediate location reachable by the left arm, and the left arm completes the task. Algorithm 3 presents the pseudocode used to execute this task.

Algorithm 3 Rearrangement of Objects on a Table

initialization; Generating inversekinematics for both arm and grasping database

pre-check; Which object can be manipulated with which arm.

```
while AllObjectPlaced != True do
    pick a random object
    if LeftArmCanManipulate = True then
        while validgrasp != None do
            if IKSolution = True then
                Grasp The Object!
            else
                check for the next validgrasp
            end
        end
    else
        manipulate the object with Right Arm
    end
end
```

In Figure 5.2 Snapshot 1, CoCoA determines which objects it can manipulate with which arm. In Snapshots 2–4, CoCoA manipulates objects by using its left arm without any assist. Snapshots 5–6 illustrate how the right arm assist the left arm to perform the task.

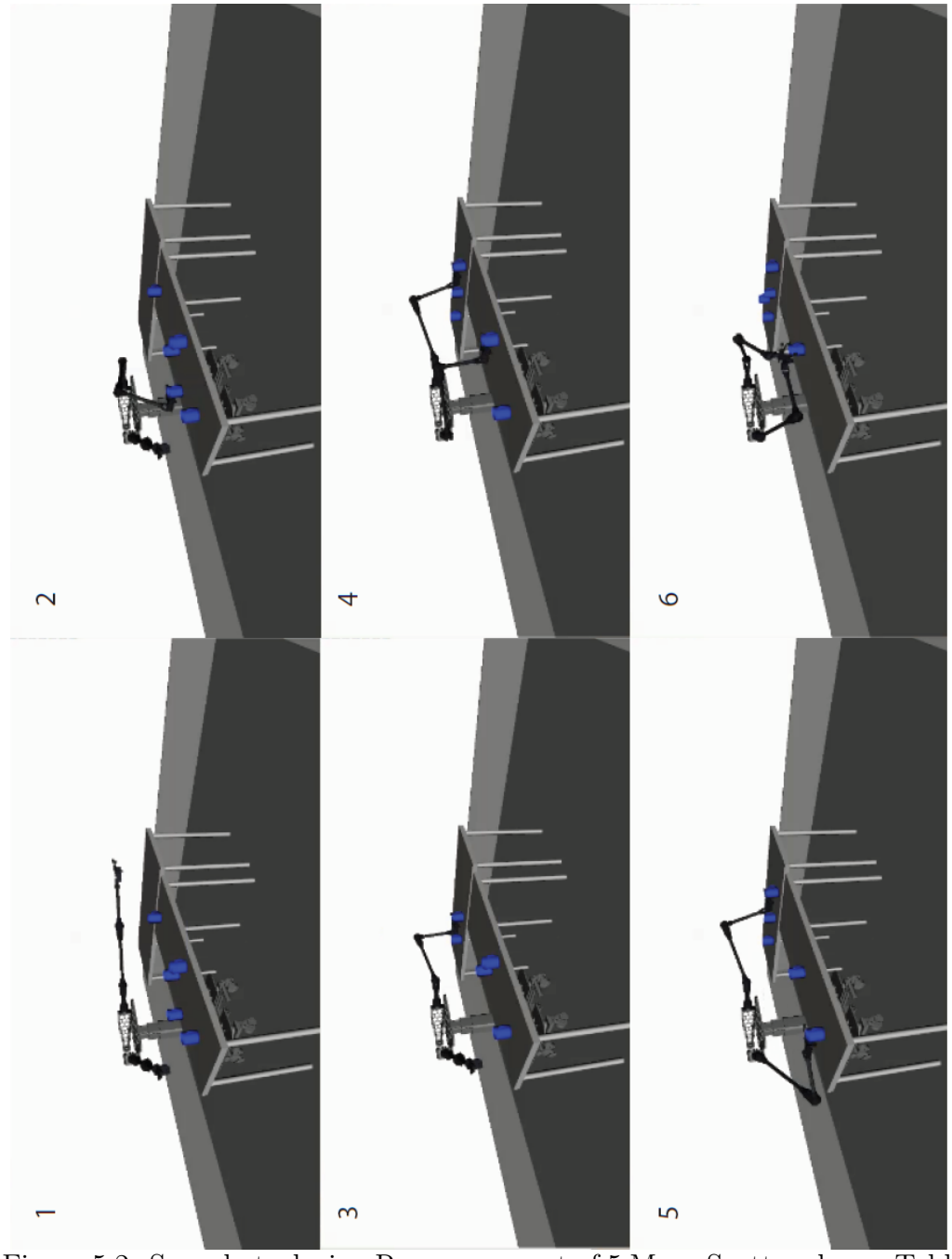

Figure 5.2: Snapshots during Rearrangement of 5 Mugs Scattered on a Table

Figure 5.2 presents snapshots taken during dynamic simulation of the rearrangement task.

5.3 Scenario 3: Mobile Manipulation Task

In this scenario, CoCoA is expected to set-up a table and the holonomic base of CoCoA is allowed to move. In Figure 5.3, a knife is missing on the table at the initial configuration. To execute the task, using the inverse reachability database, CoCoA finds a valid pose of its base to grasp the knife on the shelf and then computes a collision-free navigation plan to that base location using RRT algorithm. Once CoCoA arrives at the destination, it performs the grasp action as in the previous scenarios. To place the grasped knife on the table, another feasible base location is computed through use of the inverse reachability database; and a collision-free navigation plan is calculated. Once CoCoA assumes this base configuration, its uses its arm to places the knife on the table, as done in the previous scenarios.

In Figure 5.3 Snapshot-1, CoCoA determines a collision-free navigation plan that allows CoCoA to get the missing knife. In Snaphots 2–3, CoCoA executes that navigation plan. CoCoA gets the missing knife which is placed on the shelf in Snapshot 4. In Snapshot 5, CoCoA finds and executes another navigation plan which is used for placing the knife on the table. In the Snapshot 6 CoCoA places the knife on the table.

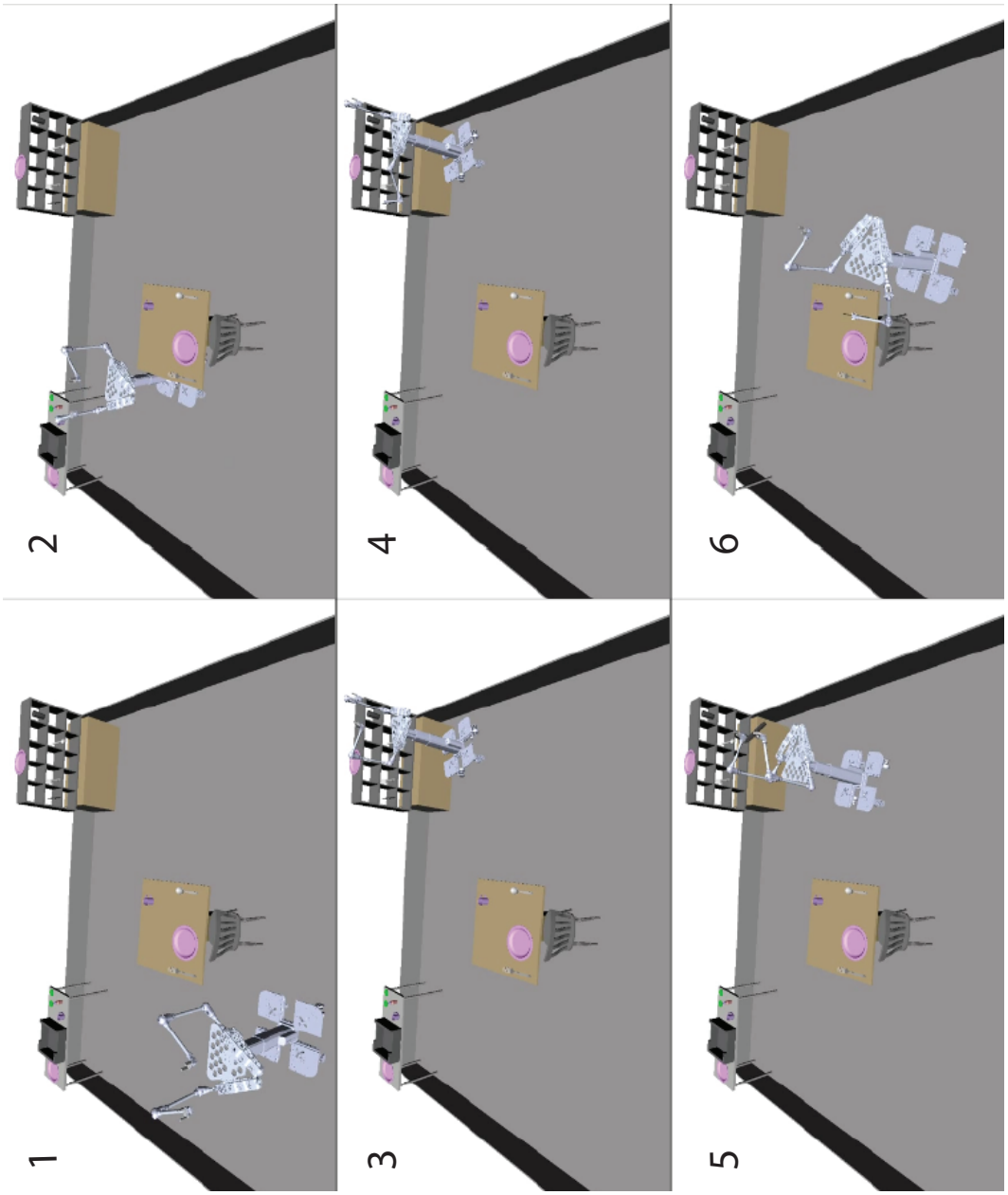

Figure 5.3: Snapshots during Mobile Manipulation of Objects

Figure 5.3 presents snapshots taken during dynamic simulation of the mobile manipulation task.

5.4 Physical Implementation: Reaching Task

CoCoA has been used for a reaching task in physical environment. Simply, kinematically-feasible and collision-free trajectories are generated for each joint. In Figure 5.4 Snapshots 1–6, CoCoA executes these trajectories to reach the object.

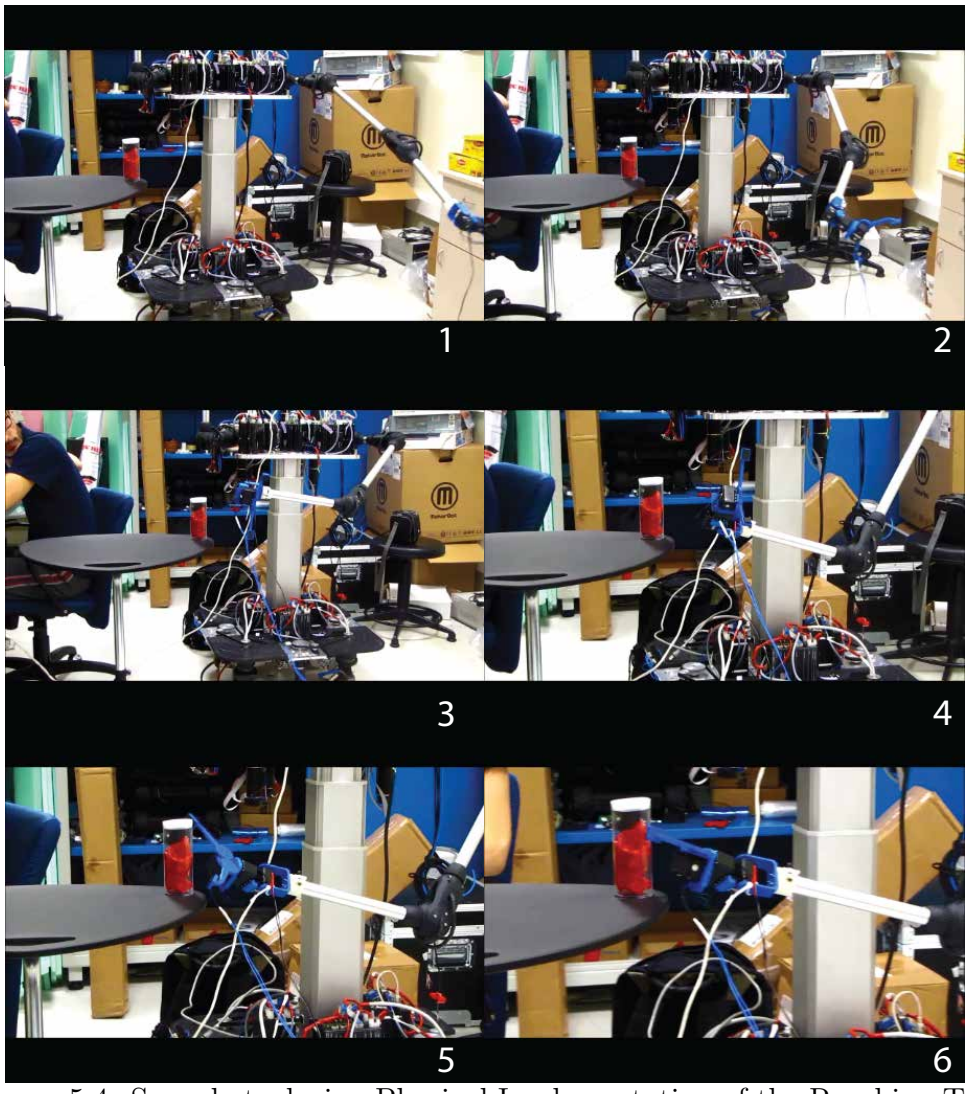

Figure 5.4: Snapshots during Physical Implementation of the Reaching Task

Chapter VI

6 Conclusion & Future Works

We have designed human-friendly arms for CoCoA robot in such a way that each arm weighs less than 1.6 kg and features 7 DoF anthropomorphic kinematics with a spherical wrist. Arms are designed to be safe even under collisions with human users and the risk of serious injury under such collisions is kept less than 0.1%. To achieve a lightweight design, we have used Bowden-cable based transmission for the first 5 DoF, which allowed us to ground the actuators. Furthermore, arms are designed to be passively back-driveable thanks to low friction due to minimal use of Bowden-cable shields.

We have also designed a holonomic base for CoCoA which is compatible with wheelchair accessible environments. The holonomic base is equipped with four steered and driven wheels to assure good traction and localization performance. Moreover, we have implemented a passive velocity field controller to enable human collaborative contour tracking tasks and to comply with human movements under physical interaction.

For software integration, kinematic/dynamic/geometric models of CoCoA have been established and inverse kinematics, stable grasp, kinematic reachability and inverse reachability databases are generated. These databases enable computation of kinematically-feasible collision-free motion/grasp plans for the arms/grippers and navigation plans for the holonomic base at in-

teractive rates. Several use scenarios of CoCoA have been demonstrated through dynamic simulations. Motion/navigation plans are computed for kinematically-feasible collision-free joint trajectories and these trajectories have been integrated with real-time feedback controllers through EtherCAT/RS-485 fieldbus communication. The applicability of the overall planning and control framework is also demonstrated through physical implementations of several case studies.

While we have designed, controlled and implemented a human-friendly CoCoA robot, there are several aspects that needs to be developed to as a part of future work to increase the performance and effectiveness of CoCoA. CoCoA should be equipped with

- perception modules (such as RGB-D sensors) that will allow it to perceive the environment and to perform object detection,
- laser range scanners to implement simultaneous localization and mapping (SLAM), and
- high-level reasoning abilities and execution-monitoring algorithms to be furnished with cognitive capabilities and to achieve full autonomy.

References

[1] S. Haddadin, A. Khoury, T. Rokahr, S. Parusel, A. Burgkart, R.and Bicchi, and A. Albu-Schaffer, "On making robots understand safety: Embedding injury knowledge into control," *International Journal of Robotics Research*, vol. 31, pp. 1578–1602, 2012.

[2] A. Albu-Schaffer, O. Eiberger, M. Grebenstein, S. Haddadin, C. Ott, T. Wimbock, and S. Wolf, "Soft robotics," *IEEE Robotics and Automation*, vol. 15, no. 3, pp. 20–30, 2008.

[3] M. Zinn, O. Khatib, B. Roth, and J. Salisbury, "Playing it safe," *IEEE Robotics and Automation Magazin*, vol. 11, no. 2, pp. 12–21, 2004.

[4] V. Duchaine, N. Lauzier, and C. ve Gosselin, *On the Design of Human-Safe Robot Manipulators*. Intech, 2010, pp. 420–435.

[5] M. Vermeulen and M. Wisse, "Intrinsically safe robot arm: Adjustable static balancing and low power actuation," *International Journal of Social Robotics*, 2010.

[6] S. Haddadin, A. Albu-Schaffer, and G. Hirzinger, "Safe physical human-robot interaction: measurements, analysis and new insights," in *Proc. of ISRR*, 2007, pp. 439–450.

[7] S. Haddadin, A. Albu-SchÃffer, and G. Hirzinger, "Safety evaluation of physical human-robot interaction via crash testing," in *Proc. of RSS*, 2007.

[8] C. Ott, O. Eiberger, W. Friedl, B. Bauml, U. Hillenbrand, C. Borst, A. Albu-Schaffer, B. Brunner, H. Hirschmuller, S. Kielhofer, R. Konietschke, M. Suppa, T. Wimbock, F. Zacharias, and G. Hirzinger, "A humanoid two-arm system for dexterous manipulation," in *Proc. of HUMANOIDS*, 2006, pp. 276–283.

[9] A. Albu-Schaffer, S. Haddadin, C. Ott, A. Stemmer, T. Wimbock, and G. Hirzinger, "The dlr lightweight robot lightweight design and soft robotics control concepts for robots in human environments," *Industrial Robot Journal*, vol. 34, no. 2, pp. 2–3, 2007.

[10] A. Albu-Schaffer, C. Ott, and G. Hirzinger, "A unified passivity based control framework for position, torque and impedance control of flexible joint robots," *International Journal of Robotics Research*, vol. 26, no. 1, pp. 23–39, 2007.

[11] ——, "A passivity based cartesian impedance controller - part ii: Full state feedback, impedance design and experiments," in *Proc. of ICRA*, 2004.

[12] C. Ott, A. Albu-Schaffer, A. Kugi, S. Stramigioli, and G. Hirzinger, "A passivity based cartesian impedance controller for flexible joint robots - Part I: Torque feedback and gravity compensation," in *Proc. of ICRA*, 2004.

[13] A. Albu-Schaffer, C. Ott, and G. Hirzinger, "A passivity based cartesian impedance controller for flexible joint robots - Part II: Full state feedback, impedance design and experiments," in *Proc. of ICRA*, 2004.

[14] M. Pratt, G. ve Williamson, "Series elastic actuators," in *Proc. of IEEE/RSJ Int. Conf. Intell. Robots Syst.*, 1995, pp. 399–406.

[15] D. Robinson, "Design and analysis of series elasticity in closed-loop actuator force control," Ph.D. dissertation, Massachusetts Institute of Technology, 2000.

[16] H. Vallery, J. Veneman, E. van Asseldonk, R. Ekkelenkamp, M. Buss, and H. van Der Kooij, "Compliant actuation of rehabilitation robots," *IEEE Robotics and Automation Magazin*, vol. 15, pp. 60–69, 2008.

[17] K. Wyrobek, E. Berger, and K. Van der Loos, H.F.M. nad Salisbury, "Towards a personal robotics development platform: Rationale and design of an intrinsically safe personal robot," in *Proc. of ICRA*, 2008.

[18] M. Zinn, "A new actuation approach for human-friendly robotic manipulation," Ph.D. dissertation, Stanford University, 2005.

[19] W. Townsend and J. Guertin, "Teleoperator slave - WAM design methodology," 1999.

[20] S. Srinivasa, D. Ferguson, C. Helfrich, D. Berenson, A. Collet, R. Diankov, G. Gallagher, G. Hollinger, J. Kuffner, and M. VandeWeghe, "Herb: A home exploring robotic butler," 2009.

[21] W. Townsend, "The effect of transmission design on force-controlled manipulator performancel," Ph.D. dissertation, Massachusetts Institute of Technology, 1988.

[22] D. Gao and C. Wampler, "Head injury criterion," *Robotics Automation Magazine, IEEE*, vol. 16, no. 4, pp. 71–74, December 2009.

[23] D. L. W. P. Davies Peter, Reaud Yvan, "Mechanical behaviour of hmpe and aramid fibre ropes for deep sea handling operations. ocean engineering," vol. 38, 2011, pp. 17–18.

[24] *Epos3 ethercat position controller, Firmware Specifications*, MaxonMotor.

[25] "Use of matlab/simulink in automation technology," Website, 2012, last checked: 05.08.2014. [Online]. Available: http://infosys.beckhoff.com/english.php?content=../content/1033/tcinfosys3/html/startpage.htm&id=

[26] "AX-18F/ AX-18A e-manual," Website, 2010, last checked: 05.08.2014. [Online]. Available: http://support.robotis.com/en/product/dynamixel/ax_series/ax-18f.html

[27] P. R. Giordano, M. Fuchs, A. Albu-Schaffer, and G. Hirzinger, "On the kinematic modeling and control of a mobile platform equipped with steering wheels and movable legs," in *Robotics and Automation, 2009. ICRA '09. IEEE International Conference on*, May 2009, pp. 4080–4087.

[28] P. Y. Li and R. Horowitz, "Passive velocity field control (pvfc): Part i - geometry and robustness," *IEEE Transactions on Automatic Control*, vol. 46, p. 2001, 2001.

[29] A. Erdogan, A. Satici, and V. Patoglu, "Passive velocity field control of a forearm-wrist rehabilitation robot," in *Rehabilitation Robotics (ICORR), 2011 IEEE International Conference on*, June 2011, pp. 1–8.

[30] A. Erdogan and V. Patoglu, "Slacking prevention during assistive contour following tasks with guaranteed coupled stability," in *Intelligent Robots and Systems (IROS), 2012 IEEE/RSJ International Conference on*, Oct 2012, pp. 1587–1594.

[31] P. Li and R. Horowitz, "Passive velocity field control (pvfc). part ii. application to contour following," *Automatic Control, IEEE Transactions on*, vol. 46, no. 9, pp. 1360–1371, Sep 2001.

[32] ——, "Passive velocity field control of mechanical manipulators," *Robotics and Automation, IEEE Transactions on*, vol. 15, no. 4, pp. 751–763, Aug 1999.

[33] J. Morenon-Valenzuela, "On passive velocity field control of robot arms," in *Decision and Control, 2006 45th IEEE Conference on*, Dec 2006, pp. 2955–2960.

[34] R. Diankov, "Automated construction of robotic manipulation programs," Ph.D. dissertation, Carnegie Mellon University, Robotics Institute,

August 2010. [Online]. Available: http://www.programmingvision.com/rosen_diankov_thesis.pdf

[35] "Ikfast: The Robot Kinematics Compiler," Website, 2006, last checked: 05.08.2014. [Online]. Available: http://openrave.org/docs/latest_stable/openravepy/ikfast/

[36] "Grasping module," Website, 2006, last checked: 05.08.2014. [Online]. Available: http://openrave.org/docs/latest_stable/openravepy/databases.grasping/

[37] "kinematicreachability module," Website, 2006, last checked: 05.08.2014. [Online]. Available: http://openrave.org/docs/latest_stable/openravepy/databases.kinematicreachability/

[38] "Inversereachability module," Website, 2006, last checked: 05.08.2014. [Online]. Available: http://openrave.org/docs/latest_stable/openravepy/databases.inversereachability/

[39] S. M. Lavalle, "Rapidly-exploring random trees: A new tool for path planning," Tech. Rep., 1998.